DOI: 10.1021/ma902820a

Macromolecules
ARTICLE

Chain Motion in Nonentangled Dynamically Asymmetric Polymer Blends: Comparison between Atomistic Simulations of PEO/PMMA and a Generic Bead−Spring Model

Martin Brodeck,*,† Fernando Alvarez,‡,§ Angel J. Moreno,‡ Juan Colmenero,‡,§,∥ and Dieter Richter†

†*Institut für Festkörperforschung, Forschungszentrum Jülich GmbH, D-52425 Jülich, Germany,* ‡*Centro de Física de Materiales (CSIC, UPV/EHU) and Materials Physics Center MPC, Paseo Manuel de Lardizabal 5, 20018 San Sebastian, Spain, and* §*Departamento de Física de Materiales, UPV/EHU, Apartado 1072, 20080 San Sebastián, Spain, and* ∥*Donostia International Physics Center, Paseo Manuel de Lardizabal 4, 20018 San Sebastián, Spain*

Received October 2, 2009; Revised Manuscript Received February 10, 2010

ABSTRACT: The polymer blend of polyethyleneoxide (PEO) and polymethylmethacrylate (PMMA) constitutes a miscible blend of high dynamical asymmetry; that is, the fully miscible components exhibit a large difference in their glass-transition temperatures, which are 200 K apart. To get a deeper understanding of the unusual PEO dynamics in this system, we have performed a fully atomistic MD simulation. Here we present all information and results obtained on the chain self-motion. We present the mean square displacements and the associated non-Gaussian parameters as a function of temperature. The associated self-correlation function is compared thoroughly with experiments. We display a Rouse analysis and find strongly modified mode friction coefficients but restoring forces that are identical to the pure melt. Thereby, the Rouse correlators are strongly stretched, and the mode number, p, dependence of the relaxation times deviates strongly from the p^{-2} Rouse behavior. We have also carried out simulations of a simple bead−spring blend, which exhibits the same qualitative dynamic features of the PEO/PMMA system. This suggests that such features are not specific of the PEO/PMMA system, but they are generic in real polymer blends with strong dynamic asymmetry. A further important issue was the test of different models that have been invoked to explain the anomalous PEO dynamics. We compare with a generalized Langevin equation (GLE) approach and with a random Rouse model dealing with a random distribution of friction coefficients. In all aspects, the GLE model agrees qualitatively very well with the results of the fully atomistic simulations. The random Rouse model may be considered to be a phenomenological instantaneous approximation valid for the case where the density fluctuations of the slow PMMA components are relaxing much slower than the relevant PEO dynamics.

I. Introduction

Blends based on thermodynamically miscible polymers are one of the most efficient and economical means to create new materials with tailored properties. Therefore, the dynamical behavior of each component in binary polymer blends has attracted increasing interest, and the question of the dynamic miscibility, that is, how exactly the molecular motions of each component in a miscible blend are modified by blending, has come into focus; see, for instance, the recent reviews[1,2] and the extended list of references therein. By now, dynamic heterogeneity is a well-established feature of polymer blends, which refers to the observation of two different characteristic time scales for segmental α-relaxation, each of them corresponding to the dynamics of one component modified by blending. (See representative refs 3−7.) A large experimental effort has been devoted to the phenomenological characterization of this effect and, by now, it is commonly accepted that this heterogeneous behavior to a large extent is a consequence of the increased local concentration of a given segment around itself due to chain connectivity.[8,9] We note that the existence of dynamic heterogeneity in blends invokes the existence of two different glass transitions as well, which, in the Lodge and MacLeish terminology are called the "effective glass-transition", T_g^{eff}, of each of the two components in the blend.[10,11] The dynamic heterogeneity also induces a dynamic asymmetry in the blend system, which can be defined as the ratio between the α relaxation times of both components A and B in the AB blend: $\Delta = \tau^{A/AB}/\tau^{B/AB}$. (In the following, A and B will denote, respectively, the slow and fast components.) Taking into account the usual non-Arrhenius temperature dependence of $\tau^{A/AB}$ and $\tau^{B/AB}$ (Vogel−Fulcher-like), it is evident that the so-defined dynamic asymmetry strongly depends on temperature. In the high-temperature limit $\tau^{A/AB} \approx \tau^{B/AB}$, and thereby $\Delta \rightarrow 1$. However, as the temperature decreases, Δ dramatically increases as the component A (slow) in the blend becomes more and more frozen, approaching its effective glass transition in the blend. Concerning the dynamics of the B component, this implies that there would be some kind of crossover from the high-temperature behavior, corresponding to the blend system in "equilibrium", toward a low-temperature regime where the B component will move within some kind of frozen matrix imposed by the A component, which, eventually, could lead to the emergence of confinement effects on the B dynamics. We can expect that these effects will be magnified significantly if the starting components of the blend exhibit very different glass-transition temperatures (ΔT_g) in their pure homopolymer state and when the composition of the blend is rich in the slow component (composition asymmetry). The first experimental evidence of extreme asymmetries including confinement effects was reported from dielectric spectroscopy studies for

*Corresponding author. E-mail: m.brodeck@fz-juelich.de.

 Published on Web 02/19/2010

polyvinylmethylether (PVME; T_g(PVME) = 249 K) blends with high concentrations of polystyrene (PS; T_g(PS) = 373 K).[12]

To characterize fully the dynamics of the fast component in asymmetric polymer blends, space/time resolution at the molecular level is needed, which is offered by neutron scattering techniques. They furthermore facilitate the selective study of either of the blend components by deuteration of the other component. This strategy has been repeatedly used to investigate the segmental α-relaxation of blend components in miscible blends. The first direct microscopic observation by these techniques of segmental dynamics under extreme asymmetry conditions was realized on a poly(ethylene oxide) (PEO) blended with poly(methyl methacrylate) (PMMA), with PEO being the minority component.[13] In this system, where the glass-transition temperatures of the two components differ by almost 200 K, a strong decoupling between PEO and PMMA dynamics was previously reported by NMR techniques.[14−16] The PEO component in the PEO/PMMA system was studied by quasielastic neutron scattering (QENS) applying different instruments providing a broad dynamic range.[13,17,18] In this way, a dramatically stretched, quasi-logarithmic relaxation dynamics was revealed, which extends from the picosecond to the hundred nanosecond scale. For an interpretation, very broad distributions of relaxation times with a T-dependent width were invoked to describe the experimental results. These broad distributions in the dynamics of the fast component could be understood as a consequence of the nonequilibrium situation reached by the fast component in the vicinity of the effective $T_{g,eff}$ of the slow-component in the blend. There, the chain and segmental dynamics of the slow-component ("matrix") could be considered to be completely frozen on the time scale of the segmental motions of the fast component. In that situation, localized and rather heterogeneous motions of the fast component can be expected. Extremely broad distributions of relaxation times were also reported for PEO in blends with PMMA under different concentrations of PEO (10−30%) from a QENS investigation of García Sakai et al.[18] There, the concept of local composition was emphasized as a key ingredient for the PEO dynamics. In another study of that group, the collective dynamics of a fully deuterated blend (dPEO/dPMMA) was addressed by means of neutron spin echo.[19] The analysis of the structure factor in terms of stretched exponentials resulted in very small stretching parameters. We note that those experiments are not selective for the PEO component in the blend, and the interpretation of the results is thus extremely difficult without the help of, for example, molecular dynamics (MD) simulation to disentangle the different contributions to the structure factor. Strong dynamic asymmetry, including confinement effects, was also found in a selective QENS investigation of the hPEO/d-polyvinylacetate (PVAc, 20/80%), where ΔT_g is ∼100 K.[20] In that work, the results showed the existence of a crossover temperature located at 70 K above the calorimetric T_g of the blend: at high temperatures, the PEO behavior is rather close to that expected for a "standard" glass-forming system in supercooled regime, whereas signatures of confined dynamics were observed when decreasing the temperature toward the average T_g of the blend. Studying the viscoelastic and dielectric relaxation behavior of the PEO/PVAc has yielded similar results.[21] The same was also found for the PEO dynamics in blend with deuterated polyethersulfone (PES), where ΔT_g is ∼180 K.[22]

Dynamic features of polymer blends have also been investigated by MD simulations (see, e.g., refs 12 and 23−31), although in most of the cases, results are reported for situations of weak or moderate dynamic asymmetry. The segmental α-relaxation in the case of strong dynamic asymmetry has been recently investigated by MD in a simple bead spring model of binary polymer blends.[30] Anomalous behavior for the fast B component has been reported. The results obtained were interpreted in terms of the mode coupling theory (MCT), suggesting the possibility of a higher-order MCT transition for the fast component dynamics. In such a scenario, the origin of this situation could be attributed to the competition between two mechanisms for dynamic arrest: intermolecular packing and confinement effects due to the freezing of the slow component.

The larger scale dynamics of the PEO component in a PEO/PMMA blend has recently been addressed looking on the single chain dynamic structure factor of PEO by neutron spin echo (NSE) spectroscopy.[17] Thereby, the range of observation was extended toward larger length and time scales. In that work, it was shown that a distribution of relaxation times derived from an observation on local scales (high Q neutron scattering experiment) suffices to describe the retarded dynamics on larger scales. The measured time distribution was converted into a distribution of friction coefficients and then inserted into a random Rouse model, the solution of which gave rise to a dynamic structure factor agreeing with the data. Thereby, the experimental situation corresponded to that of a frozen PMMA matrix in which the PEO was moving. (The time scale of PMMA motion was far outside the observation window of the NSE instrument.)

Prior to that, experiments on translational diffusion on a short PEO chain in a PMMA matrix using forced Rayleigh scattering[32] revealed a very low diffusion coefficient corresponding to an associated effective friction coefficient that would be five orders of magnitude slower than those revealed by the NSE data on the scale of the chain. Therefore, the global dynamics expressed by the chain diffusion senses very deep traps retarding the motion dramatically.

In a recent work, some of us have also investigated chain dynamics in a generic, simple bead−spring model for nonentangled polymer blends.[31] Computer simulations of such a model have revealed novel features for the relaxation of the Rouse modes of the fast component. Therefore, by increasing the dynamic asymmetry in the blend to intensify confinement effects on the fast component, the latter exhibits a crossover in the wavelength dependence of the relaxation times of the Rouse modes. At high temperature, the Rouse scaling expected for nonentangled chains is found for both components. By decreasing the temperature, however, strong deviations are found for the fast component. This crossover for the nonentangled fast component by increasing dynamic asymmetry has also been observed in simulations[33−35] of homopolymers by increasing the chain length beyond the entanglement length. For the latter case, this behavior has been rationalized[36] by a generalized Langevin equation approach. In this framework, a slow memory kernel arises from the slow relaxation of the density fluctuations around the entangled, tagged homopolymer chain.[36−38] For nonentangled homopolymers, such a relaxation is fast, and the original Rouse model is recovered as a limit case. In ref 31, it has been suggested that the analogous crossover observed for the fast component in the nonentangled bead−spring blend follows from the same physical picture: strong memory effects associated with slow relaxation of density fluctuations (in this case of the confining matrix formed by the slow component) around the tagged chain of the fast component.

To complement the many reported experiments on the unusual PEO dynamics and to gain a deeper understanding, we have performed a fully atomistic MD simulation on the PEO/PMMA system. In this work, we present all information obtained on the chain self-motion. Thereafter, a Rouse analysis is performed; we find strongly modified mode friction but restoring forces identical to the pure melt. Simulation results for the PEO/PMMA system are qualitatively similar to those obtained for a simple bead−spring blend model with strong dynamic asymmetry. This suggests that the observed dynamic features are general in real blends with strong dynamic asymmetry. Another important issue is the

Table 1. Simulated Densities and Cell Sizes for Different Temperatures[a]

T (K)	density ρ (g/cm^3)	size a (Å)	$< R_{ee}^2 >$ (Å^2)	$< R_g^2 >$ (Å^2)	$< R_{ee}^2 > / < R_g^2 >$
300	1.1157	41.220	1199	169	7.09
350	1.0891	41.552	1136	170	6.68
400	1.0589	41.944	997	171	5.83
500	0.9977	42.784	879	152	5.78

[a] Values of the average mean squared end-to-end distance and radius of gyration for the PEO chains in the blend are also included.

test of different models invoked to explain the anomalous dynamics. We explicitly compare with a generalized Langevin equation (GLE) approach and with a random Rouse model (RRM).

The article is structured as follows: In Section II, we discuss the details of the simulation approaches taken, the fully atomistic MD simulation, and the coarse-grained bead and spring model featuring beads with different interaction potentials. The theoretical framework is introduced in Section III. In Section IV, we present the results of the fully atomistic model and summarize the outcome of the bead spring simulations. Section V is devoted to the Rouse analysis of both simulation approaches. It is shown that the generic bead spring model may be mapped to the fully atomistic simulations. In Section VI, we discuss the results and scrutinize both the GLE and the RRM approaches. Finally, in Section VII, conclusions are drawn.

II. Simulation Method

A. Fully Atomistic Simulations of PEO/PMMA. The simulations presented in this article were carried out using the software package Materials Studio 4.1 and the Discover-3 module (version 2005.1) from Accelrys with the COMPASS forcefield (condensed-phase optimized molecular potentials for atomistic simulation studies). More information about this force field, including the complete analytical expression for the functional form, can be found in refs 39 and 40. Coulombic and van der Waals interactions have been approximated by a group-based spherical cutoff method. Previous investigations of PEO using the COMPASS forcefield have shown that a choice of 12 Å for the cutoff radius and the spline region yields excellent agreement with experimental results.[41] We have chosen the same parameters for the simulation of PEO/PMMA. This procedure allows a direct comparison between the results obtained for pure PEO and those corresponding to PEO in the PEO/PMMA blend.

The simulated system was created using the Amorphous Cell protocol, which is based on an extension of the method proposed for the first time by Theodorou and Suter.[42,43] A cubic cell containing five polymer chains of 43 monomer units of ethylene oxide and 15 polymer chains of 25 monomer units of methyl methacrylate was constructed at 400 K under periodic boundary conditions resulting in a cell with 7170 atoms. The density at this temperature was determined by simulation of the system under NPT conditions for 2 ns under atmospheric pressure. After the creation of the cell, standard minimization procedures (Polak-Ribière conjugated gradients method) were followed to minimize the so-obtained energy structure, and a subsequent dynamic run was performed for 2 ns to equilibrate the sample. The system obtained in this way was used as a starting point for collecting data during MD runs of different duration. As integration method, we have used the velocity Verlet algorithm with a time step of 1 fs. The simulations were carried out in the NVT ensemble. The velocity scaling procedure with a temperature window of 10 K was used to control the temperature. First of all, we carried out a first MD run of 1 ns, collecting data every 0.01 ps. After that, two more successive runs of 2 and 100 ns (200 ns for $T = 300$ K) were carried out, collecting data every 0.05 and 0.5 ps respectively. No signatures of "aging processes" were detected between successive runs, assuring equilibrium behavior of the simulated cell. The same system was used to yield corresponding cells at different temperatures, namely, 300, 350, and 500 K. The NPT simulation as described above was carried out at each of these temperatures. The obtained densities and cell sizes are listed in Table 1. To our knowledge, the only available experimental values for the density of PEO/PMMA blend, in the composition used by us, were reported by Martucelli et al.[44] The reported values correspond to polymer films of PEO/PMMA, where the molecular weight of the two components was very different from that simulated by us. Moreover, the experimental values correspond to three temperatures that do not coincide with those of the simulations. Although the temperature dependence of the density obtained by NPT follows a similar trend as that of the experimental data, the absolute values are on the order of 4% lower than the experimental ones. Similar deviations have been observed in other atomistic simulations of polymers (in particular bulky polymers), and they are likely related to the limitations of the force fields.

Table 1 also shows the averaged mean squared end-to-end distance, $< R_{ee}^2 >$, the radius of gyration, $< R_g^2 >$, and the ratio between both for the PEO chains in the simulated blend. First of all, we can see that $(< R_{ee}^2 >)^{1/2}$ is always smaller than the size of the cell and that $(< R_g^2 >)^{1/2}$ is about three times smaller than that size. This should prevent the system from significant interaction of a chain with its periodic images. A similar criterion has been followed by different authors (see, e.g., refs 34, 35, and 45.) Table 1 shows that the ratio $< R_{ee}^2 > / < R_g^2 >$ is close to 6 at high temperature, indicating Gaussian statistics of the chains. (Using the correct expression and $N = 43$, a factor of 5.87 is expected for Gaussian chains.) As soon as the temperature decreases, we observe a tendency to deviate from the Gaussian behavior.

B. Bead Spring Simulations. MD simulations of bead−spring models for polymer blends with strong dynamic asymmetry were reported in ref 30. The model used here introduces a mixture A/B of bead−spring chains with the same number of monomers, $N = 21$. The latter reduces to the B homopolymer for a zero fraction of A chains. The monomer mass is $m = 1$. Monomers within a same chain are identical (of the same species A or B). The monomer−monomer interaction potential is

$$V_{\alpha\beta}(r) = 4\varepsilon\left[\left(\frac{\sigma_{\alpha\beta}}{r}\right)^{12} - \frac{7}{c^{12}} + \frac{6}{c^{14}}\left(\frac{r}{\sigma_{\alpha\beta}}\right)^{2}\right]$$

where $\varepsilon = 1$, $c = 1.15$, and $\alpha,\beta \in \{A,B\}$. Potential and forces are continuous at the cutoff $r_c = c\sigma_{\alpha\beta}$. The interaction diameters are $\sigma_{BB} = 1$, $\sigma_{AA} = 1.6\sigma_{BB}$, and $\sigma_{AB} = 1.3\sigma_{BB}$. Chain connectivity is introduced by a FENE potential[34]

$$V_{\alpha\alpha}^{\mathrm{FENE}}(r) = -kR_0^2\varepsilon \ln\left[1 - \frac{r^2}{(R_0\sigma_{\alpha\alpha})^2}\right]$$

between consecutive monomers, with $k = 15$ and $R_0 = 1.5$. The blend composition is $x_B = N_B/(N_A + N_B)$, where N_α is the number of α monomers. The total number of monomers changes between 1470 and 9975 for, respectively, the smallest and largest simulated cells. We use a fixed packing fraction $\phi = (\pi/6V)[N_A\sigma_{AA}^3 + N_B\sigma_{BB}^3] = 0.53$ both for the blend and the B homopolymer, where V is the simulation cell volume. For the blend, we use a composition $x_B = 0.3$.

Temperature, T, distance, wave vector, Q, and time, t, are measured, respectively, in units of ε/k_B, σ_{BB}, σ_{BB}^{-1}, and $\sigma_{BB}(m/\varepsilon)^{1/2}$. We use a time step between 5×10^{-4} and 5×10^{-3} for, respectively, the highest and lowest T. Equations of motion are integrated in the velocity Verlet scheme.[46] Thermalization at the requested T is achieved by periodic velocity rescaling. Once equilibrium is reached, production runs are performed in the microcanonical ensemble, with 20−40 independent runs for statistical averages. The longest production runs extend up to 400 million time steps.

III. Theoretical Framework

A. Rouse Model. The dynamics of a generic linear, ideal Gaussian chain of N monomers (in the following referred as the "tagged chain") is the starting point and standard description for the Brownian dynamics in polymer melts.[47] The Rouse model starts from a Gaussian chain representing a coarse-grained polymer model, where springs represent the entropic forces between hypothetic beads. The chain segments are subject to an entropic force $\propto 3k_BT/l^2$ (k_B: Boltzmann constant, T: temperature, l: statistical bead size) and an effective stochastic force $f(n,t)$, representing the interactions exerted by the surrounding chains that fulfills $\langle f(n,t)\rangle = 0$ and $\langle f_\alpha(n,t)\, f_\beta(m,0)\rangle = 2k_BT\zeta_0\, \delta_{nm}\, \delta_{\alpha\beta}\, \delta(t)$; ζ_0 denotes a friction coefficient, and α,β are the Cartesian components. With this, the Langevin equation for segment motion assumes the form

$$\zeta_0 \frac{\partial x(n)}{\partial t} = \frac{3k_BT}{\ell^2}[x(n+1) - 2x(n) + x(n-1)] + f_x(n,t) \quad (1)$$

The Langevin equation is solved by introducing normal coordinates (Rouse modes)

$$X_p(t) = N^{-1}\sum_{i=1}^{N} r_i(t)\cos[(i-1/2)p\pi/N]$$

with modes $p = 0, 1, ..., N-1$. The mode $p = 0$ corresponds to the chain center of mass diffusion $D_R = k_BT/(N\zeta_0)$. Modes with $p > 0$ are described by Rouse mode correlators

$$\langle X_p(t)X_q(0)\rangle = \frac{\ell^2}{8N\sin^2(p\pi/2N)}\exp\left(-\frac{t}{\tau_p}\right)\delta_{p,q} \quad (2)$$

with the mode relaxation time

$$\tau_p = \frac{\zeta_0\ell^2}{12k_BT\sin^2(p\pi/2N)} \approx \frac{\tau_R}{p^2}$$

B. Extensions of the Rouse Model. The present work deals with the dynamics of nonentangled fast chains in a blend with a polymer matrix that exhibits a much slower relaxation. The presence of such a slow matrix may question a fundamental assumption of the Rouse model: the purely random character of the external forces acting on the tagged chain, strong memory effects being expected. It may also suggest a broad distribution of effective friction coefficients, arising from the structural heterogeneities probed by the tagged chain in its motion along the quasistatic matrix. These two ideas are underlying in the two theoretical approaches considered in this work for the case of strong dynamic asymmetry at low temperatures: the renormalized Rouse models within the framework of generalized Langevin equations and the random Rouse model.

Generalized Langevin Equation and Renormalized Rouse Models. Now we summarize the main predictions of methods based on generalized Langevin equations for observables characterizing chain dynamics. In particular, we summarize results within the approach of renormalized Rouse models for the memory kernel. Extensive reviews can be found, for example, in refs 36−38. Let $\vec{r}(n)$ $(1 \le n \le N)$ be the monomer positions of a tagged Gaussian chain of N monomers of mass m connected by harmonic springs of constant $3k_BT/l^2$, which interacts with similar chains in a polymer melt. By using projection operator techniques, the Liouville equation of the whole system can be rewritten as a generalized Langevin equation (GLE) for the coordinates of the tagged monomers. For an isotropic system, the GLE reads

$$m\frac{d^2\vec{r}(n;t)}{dt^2} = -\frac{3k_BT}{l^2}[\vec{r}(n+1;t) - 2\vec{r}(n;t) + \vec{r}(n-1;t)] + \vec{F}^{Q}(n;t) - \sum_{k=1}^{N}\int_0^t d\tau\Gamma(n,k;t-\tau)\frac{d\vec{r}(k;t-\tau)}{dt} \quad (3)$$

The term $\vec{F}^{Q}(n;t) = \exp[iQLQt]\vec{F}(n;0)$ is the "generalized fluctuating force". In this expression, L is the Liouville operator, $Q = 1 - P$, where P is the projection operator on the tagged chain coordinates, and $\vec{F}(n;0)$ is the force exerted by the monomers of all other chains on the nth monomer of the tagged chain. Thus, $\vec{F}^{Q}(n;t)$ is the time evolution of $\vec{F}(n;0)$ through "projected dynamics" (evolution through real dynamics is given by $\exp(iLt)$).

The memory kernel is proportional to the correlator of the generalized forces, $\Gamma(n,k,t-\tau) = (6k_BT)^{-1}\langle\vec{F}^{Q}(n;0)\vec{F}^{Q}(k;t-\tau)\rangle$, and contains all of the information about the intermolecular interactions on the tagged monomer. The GLE at this point is not solvable because the fluctuating forces and the memory kernel cannot be expressed as functions of $\vec{r}(n)$ alone, and some approximations are needed to reduce eq 3 to a closed equation.

Before discussing this point, it is worth mentioning that the Rouse model is recovered as a limit case of the GLE if two conditions are fulfilled:[36−38] (i) no spatial correlations between matrix density fluctuations so that $\Gamma(n,k,t-\tau) \approx \delta_{nk}$ and (ii) fast relaxation of matrix density fluctuations around the tagged chain, so that $\Gamma(n,k,t-\tau) \approx \delta(t-\tau)$. With these conditions, we have

$$6k_BT\Gamma(n,k;t-\tau) = \langle\vec{F}^{Q}(n;0)\vec{F}^{Q}(k;t-\tau)\rangle = 6k_BT\zeta\,\delta_{nk}\,\delta(t-\tau) \quad (4)$$

where ζ is an effective friction coefficient. By inserting eq 4 in eq 3 and, as usual, neglecting the inertial term for $t \gg m/\zeta$, we recover the equations of motion of the Rouse model. In this limit, the generalized fluctuating forces play the role of the random forces of the Rouse model. They indeed follow the same correlation assumed by the Rouse model. (See eq 4.)

Now we discuss the general case of slow relaxation of the memory kernel. First, the kernel is rewritten in terms of monomer density fluctuations of the matrix around the

tagged chain[36−38]

$$\Gamma(n,k;t-\tau) = \frac{1}{6k_BT}\int\int \mathrm{d}\vec{r}\ \mathrm{d}\vec{r}'\ \vec{F}(\vec{r},n)\cdot\vec{F}(\vec{r}',k)\langle\delta\rho^{Q}(\vec{r},n;0)\ \delta\rho^{Q}(\vec{r}',k;t-\tau)\rangle \quad (5)$$

The quantity $\delta\rho^{Q}(\vec{r}',k;t-\tau)$ is the projected matrix density fluctuation at time $t-\tau$ at a distance $\vec{r}'$ from the k^{th}-tagged monomer. The interactions between matrix monomers and tagged monomers are mapped into effective hard-sphere potentials. A weighted average approximation[37] is assumed for the correlators of matrix density fluctuations, and transformation to reciprocal space (of wave vectors q) is performed. After this, the memory kernel in eq 5 takes the form

$$\Gamma(n,k;t-\tau) = \frac{C}{k_BT}\int_0^{l^{-1}} S^{Q}(q,t-\tau)\omega_{nk}^{Q}(q,t-\tau)q^4\,\mathrm{d}q \quad (6)$$

where C is a constant containing structural information.[36−38] In this expression, S^{Q} is the projected dynamic total structure factor of the matrix, and ${\omega_{nk}}^{Q}$ is the projected single-chain dynamic structure factor for the n^{th}- and k^{th}-tagged monomers. Equation 6 for the memory kernel is a general starting point for the different approximation schemes of the projected dynamics, which aim to obtain an approximate closed solvable form for the GLE (eq 3).

The projected quantities in the integrand of eq 6 are rewritten as[36]

$$S^{Q}(q,t) = S(q)\ exp[-q^2\langle\Delta r^2(t)\rangle_Q/6] \quad (7a)$$

$${\omega_{nk}}^{Q}(q,t) = \omega_{nk}(q)\ exp[-q^2\langle\Delta r n k^2(t)\rangle_Q/6] \quad (7b)$$

where $S(q)$ and $\omega_{nk}(q)$ are the corresponding static structure factor and chain form factor. A Vineyard-like approximation is assumed in eq 7a.[38] Within the approach of the renormalized Rouse model, the projected mean squared displacements (for self- and intrachain collective motions) in eqs 7a and 7b are replaced by their respective values in the Rouse model.[36] This ansatz allows us to close the GLE, which now becomes solvable. From the corresponding solutions $r(n;t)$, it is possible to compute other observables, including the real $\langle\Delta r^2(t)\rangle$ and $\langle\Delta {r_{nk}}^2(t)\rangle$. The latter can be reintroduced in eqs 7a and 7b as new approximations for the projected dynamics in successive renormalizations (which lead to the so-called n-renormalized Rouse models[36]).

The solution of the GLE equation allows us to compute any observable dependent on the coordinates of the tagged monomers, as, for example, the correlator of the Rouse modes, $\Phi_{pp}(t)$. By doing so,[36] the relaxation time of the pth mode follows, for $p/N \ll 1$, an approximate scaling $\tau_p \approx (N/p)^{5/2}$, different from the quadratic power law of the Rouse model. In the twice renormalized model, the scaling becomes $\tau_p \approx (N/p)^3$, and for the three-times renormalized model, one finds $\tau_p \approx (N/p)^{7/2}$.[36] For the monomer mean squared displacement, $\langle\Delta r^2(t)\rangle \approx t^x$, at times $t < \tau_1$. The respective anomalous exponents for one, two, and three renormalizations are[36] $x = 2/5$, $1/3$, and $2/7$, all smaller than the Rouse exponent $1/2$. Models with four or more renormalizations are physically inconsistent with approximations introduced in the memory kernel and are not considered.[36] Apart from the anomalous power-laws, renormalized models also predict a strong stretching of the Rouse correlators,[36] in contrast with the pure exponential behavior of the Rouse model.

The problem of relaxation of strongly entangled chains has been traditionally addressed mainly in the framework of the phenomenological tube model (see, e.g., ref 48). For entangled chains, matrix density fluctuations around the considered tagged chain are expected to relax slowly and to be spatially correlated. On this basis, GLE methods have aimed in the last years to provide a microscopic theory for the phenomena associated with entanglement effects.[36−38] Similar arguments may be invoked for the application of GLE methods in the physical situation investigated in this work, that is, the chain motion of the minority (nonentangled) component in a blend with a matrix that exhibits a much slower relaxation. Connections of MD simulation results in this work with the anomalous scaling laws and nonexponentiality of the Rouse modes (see above), predicted by renormalized Rouse models, are discussed in Section VI.

Random Rouse Model. In the random Rouse model, the Langevin eq 1 is generalized, allowing for randomly distributed friction coefficients

$$\frac{\partial x(n)}{\partial t} = \sum_{m=0}^{N-1} L_{nm}\left(\frac{3k_BT}{l^2}[x(m+1)-2x(m)+x(m-1)]+f(m,t)\right) \quad (8)$$

where $L_{nm} = 1/\zeta_n\delta_{nm}$ is the diagonal mobility matrix. The correlator of the stochastic forces then becomes $\langle f_\alpha(n,t)\ f_\beta(m,0)\rangle = 2k_BT\ \zeta_n\ \delta_{nm}\ \delta_{\alpha\beta}\ \delta(t)$. Note that the latter is an assumption rather different from the basis of GLE methods! Here spatial and time correlations between the external forces are fully neglected as in the original Rouse model. After transformation to bond vectors, $\vec{x}_n = \vec{x}_0 + \sum_{k=1}^{n}\vec{r}_k$, the resulting tridiagonal matrix equation can be solved semianalytically,[49] yielding eigenvalues, ε_p, and eigenvectors, a_{np}, facilitating the transformation to normal coordinates. The correlators for the bead displacements involve these eigenvectors and still feature single exponential correlation functions

$$\langle r_n(t)^2\rangle = 6\bar{D}\,t + l^2\sum_{p}^{N-1} 2c_{np}^2(1-\exp(-\varepsilon_p t)) \quad (9)$$

with $c_{np} = \sum_{k=1}^{n} a_{kp} - (1/N\bar{\zeta})\sum_{k=1}^{N-1}\bar{1}\sum_{l=1}^{N-1}\zeta_l a_{kp}$. The dispersion of ε_p now depends on the assumed distribution of the friction coefficients. Furthermore, a simple expression for the center of mass diffusion evolves

$$\bar{D} = k_BT/\sum_{n=0}^{N-1}\zeta_n = k_BT/N\bar{\zeta} \quad (10)$$

The self-correlation function $F_s(Q,t)$ then becomes

$$F_s(Q,t) = 1/N\sum_{n=0}^{N-1}\exp[-Q^2/6\langle r_n(t)^2\rangle] \quad (11)$$

The detailed results of this model naturally depend strongly on the assumed distribution of friction coefficients. As a general observation, we note that singular very high friction slows down the center of mass diffusion coefficient and the long wavelength modes strongly, whereas most of the shorter wavelength modes will stay unaffected. This model has been used for describing the single chain dynamics structure factor of PEO in PEO/PMMA blends as it is measured by neutron scattering.[17] In that case, the friction coefficients were drawn from log-normal distributions, which are characterized by a small fraction of very high

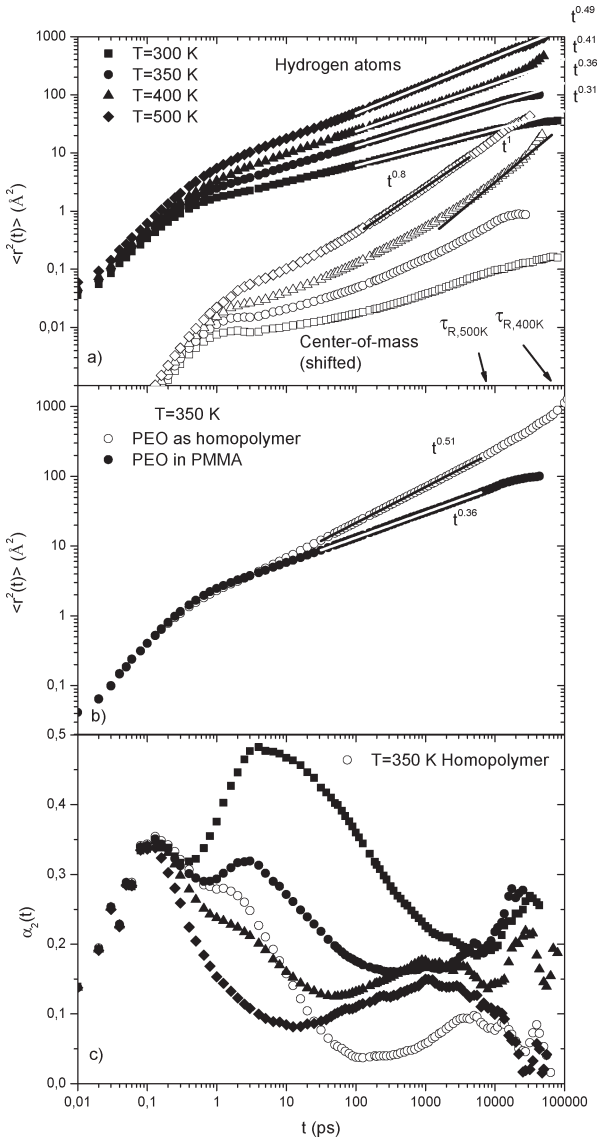

Figure 1. (a) Mean square displacement (MSD) for PEO in the blend at temperatures of 300, 350, 400, and 500 K. Lines are fits of a power law at times $100 < t < 5000$ ps. Full symbols correspond to the MSD of hydrogen atoms in the PEO chain, and empty symbols correspond to the center-of-mass motion (multiplied by a factor of 0.1). (b) Comparison of the MSD of the PEO hydrogens in the homopolymer (empty symbols) and in the blend (full symbols) at $T = 350$ K. (c) Non-Gaussianity parameter of the PEO hydrogens In addition to the four temperatures of the blend (full symbols) the values for the homopolymer at $T = 350$ K are shown (empty symbols).

friction coefficients. The employed distributions, thereby, related directly to the measured relaxation time distributions using high-spatial-resolution neutron spectroscopy.

IV. Results

A. PEO/PMMA. Figure 1 presents an overview of the results of the MD simulation for PEO/PMMA at a 20/80% weight composition for different temperatures. In Figure 1a, we display the average mean square displacements (MSD) of the PEO H-atoms for temperatures between 300 and 500 K. At times after the microscopic dynamics that dominates up to ~1 ps, the H-MSDs show a power law increase $\langle r(t)^2\rangle \approx t^x$ spanning the full simulation regime up to several 10 000 ps. Thereby the time exponent increases from $x \simeq 0.31$ at $T = 300$ K to $x \simeq 0.49$ at 500 K, corresponding closely to the prediction of the Rouse model featuring $x = 0.5$.[50] We note, however, that in particular at higher temperatures part of the increase in x may relate to the center of mass (c.m.) diffusion that becomes relatively more important with increasing T. The lower part of Figure 1a displays the c.m. MSD that undergoes a much more significant increase with T than the internal chain motion. Whereas at 300 K the c.m. MSD is nearly flat, at 500 K, $\langle r(t)^2\rangle_{cm}$ exhibits a power law increase with $x = 0.8$ very close to what is observed for short chain melts such as polybutadiene (PB)[51] and polyethylene (PE).[52] There, this observation was related to the phenomenon of interchain coupling, which is not included in the Rouse model. Finally, Figure 1a includes the Rouse times τ_R for 400 and 500 K. From their position on the time axis, we may see that except for 500 K all simulations were performed at $t \leq \tau_R$, thus focusing on the internal chain dynamics.

Figure 1b shows a direct comparison of the H-MSDs between the PEO homopolymer melt and PEO in the PMMA blend at 350 K. For short times up to ~5 ps, both MSDs agree quantitatively; at short times, even well beyond the microscopic dynamics, the PMMA matrix does not affect the PEO motion. Starting around 10 ps, the MSD of PEO in PMMA is systematically retarded compared with pure PEO reaching a factor of 4 at 10^4 ps. At even longer times, where under the influence of the c.m. diffusion the PEO MSD in pure PEO is increasing faster than the Rouse power law of $t^{0.5}$, the motions in the blend are even further slowed down and seem to bend toward a plateau in time.

In Figure 1c, we show the associated non-Gaussianity parameter $\alpha_2(t)$ measuring the leading order deviation from a Gaussian line shape of the H−self-correlation function

$$\alpha_2(t) = \frac{3\langle r^4(t)\rangle}{5\langle r^2(t)\rangle^2} - 1$$

where $\langle r(t)^n\rangle$ are the moments of the van Hove self-correlation function. For 350 K, we also include $\alpha_2(t)$ for pure PEO. A number of features are noteworthy: (1) At short times in the microscopic regime, $\alpha_2(t)$ displays a strong peak that is temperature-independent and is also present in the homopolymer melt. (2) In the intermediate time regime $1 \leq t \leq 1000$ ps, where $\alpha_2(t)$ from the homopolymer displays a shoulder for $t \leq 10$ ps before it starts to vanish nearly for longer times, PEO in the blend develops a strong second maximum that diminishes with increasing temperature and finally is absent at 500 K. (3) The most remarkable additional feature in the blend data is the increase in $\alpha_2(t)$ toward longer times above about several 1000 ps, which indicates an increase in the heterogeneity, if the PEO segments start to explore larger regions in space. We note that this apparent heterogeneity at longer times may also be related to the observed plateauing of $\langle r(t)^2\rangle$ at long times, as discussed in connection with Figure 1b.

The deviations of the van Hove self-correlation function $4\pi r^2 G_s^H(r,t)\,dr$ from the Gaussian line shape can also be directly visualized in real space. The self-part of the van Hove correlation function describes the probability of finding a hydrogen atom after time t between a distance r and $r + dr$ relative to its position at $t = 0$. As a function of time, $4\pi r^2 G_s^H(r,t)\,dr$ shifts to larger displacements and broadens. The MSDs shown in Figure 1a are obtained from $4\pi r^2 G_s^H(r,t)\,dr$ by integration

$$\langle r(t)^2\rangle = \int_0^\infty r^2\,dr\,4\pi r^2 G_s^H(r,t)$$

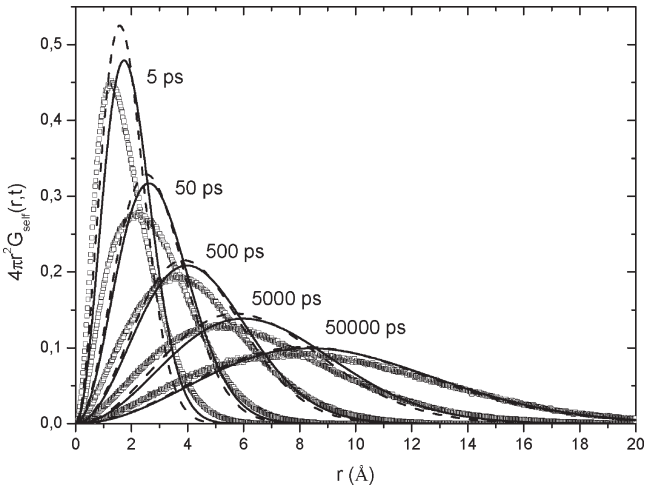

Figure 2. Van Hove self-correlation function of the PEO hydrogens in the blend, for different times (t = 5, 50, 500, 5000, and 50 000 ps) at T = 350 K. The solid curves show a Gaussian distribution with a MSD taken from Figure 1a, and the dashed curves are (normalized) fits of Gaussian distributions to the shown data points. The peaks are clearly shifted to higher times accounting for the tails in the correlation function.

In Figure 2, we compare the simulated correlation functions with the Gaussian correlation functions based on the MSDs of Figure 1a at 350 K. Compared with the simulated curves, the maxima of the strictly Gaussian functions are shifted to higher r values, and at the same time, the functions appear narrower than the simulated curves. The reason for these differences is the tails in the simulated curves that appear as a result of the heterogeneities in the blend: Some segments in a favorable environment move faster than the average, and others under unfavorable conditions are retarded compared with the average segment.

Now we move to the incoherent scattering functions $F_s(Q,t)$ in the low Q range ($0.1 < Q < 0.4$ Å^{-1}), where Rouse behavior was found for pure PEO.[41] These results are shown in Figure 3a,b. Figure 3a displays the temperature dependence of $F_s(Q,t)$ for PEO in the blend at a value of Q = 0.3 Å^{-1}, where pure PEO displays stretched exponential behavior with β = 0.5, that is, Rouse-like behavior.[50] The line shape of $F_s(Q,t)$ for PEO in the blend strongly depends on temperature. Once again, $F_s(Q,t)$ approaches Rouse-like behavior at high temperature, but as soon as the temperature decreases, deviations from that behavior become evident. First, the β value decreases with temperature approaching 0.3 at low temperature. Moreover, above ~20 ns, there are clear signatures for deviations from a simple stretched behavior. $F_s(Q,t)$ seems to display an upturn to some kind of plateau at longer times. Interestingly, there are also indications of this behavior in the MSD of PEO in the blend and even in the MSD of the chain center of mass. (See Figure 1a.) We note that this is also the time range where α_2 increases toward a possible new peak.

At 350 K, Figure 3b compares the $F_s(Q,t)$ corresponding to pure PEO and PEO in the blend for different Q values. This comparison is restricted to the low-Q range, where pure PEO follows Rouse behavior. For all Q values, the $F_s(Q,t)$ corresponding to PEO in the blend is more stretched than that for pure PEO, and thereby the relaxation time is higher. In addition, the plateau in the curves at t > 20 ns is evident for all Q values.

The self-correlation functions $F_s(Q,t)$ for all Q values and temperatures were fitted to stretched exponential functions (KWW) with β as free parameter. The fitting time range was restricted from 2 ps to 20 ns to avoid both: the microscopic

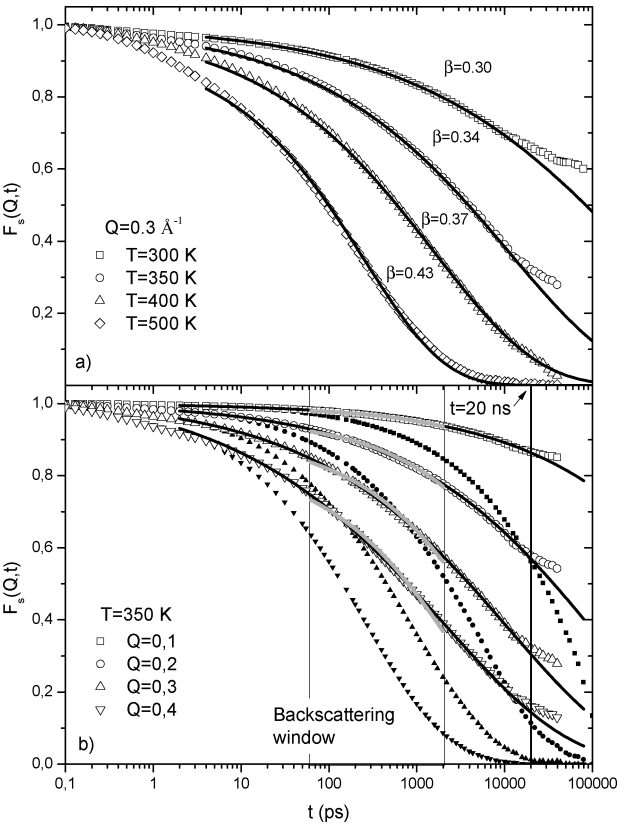

Figure 3. (a) Dynamic incoherent scattering function of PEO in PMMA at Q = 0.3 Å^{-1} for temperatures of 300, 350, 400, and 500 K. KWW fits with corresponding β values are shown. (b) Dynamic incoherent scattering function of PEO as homopolymer (full symbols) and in blend with PMMA (empty symbols) at T = 350 K. The black lines are KWW fits with variable β parameter; the gray lines are fits with β = 0.5 fixed in the time regime 60 < t < 2000 ps (backscattering window).

regime, which obviously is not related to the Rouse behavior, and the longer times, where the deviations from the stretched functional form are evident. Some of the fitting curves are included in Figure 3b. As can be seen, within the fitting range, they are good descriptions of $F_s(Q,t)$. Moreover, to compare with some previously reported experimental results, we have also carried out a second fit by using a KWW function with β = 0.5 fixed (i.e., Rouse-like) but restricting the fitting time range to a narrow regime from ~60 ps to 2 ns. This narrow regime roughly corresponds to the dynamic range covered by neutron backscattering spectrometers. In ref 17, some backscattering measurements of PEO in blends of PEO/PMMA (25/75%) were reported and analyzed using the Fourier transformation of a Rouse-like expression for $F_s(Q,t)$. Figure 3b shows that in such a restricted range, a Rouse-like description of $F_s(Q,t)$ is not in contradiction with the simulation results. However, the relaxation times obtained by means of this restricted fitting do not represent the full time decay of $F_s(Q,t)$.

Figure 4a shows the values for the β parameter obtained by means of the above-described KWW fits. As we mentioned above, the values of β decrease with temperature from values close to 0.5 (in the low Q limit) at high temperature toward values close to 0.3 at 300 K. Moreover, the obtained values corresponding to the low-temperature regime hardly depend on Q. However, in the high-temperature regime, some Q dependence seems to be evidence that, as alluded to in the context of the MSDs, to some extent may relate to the increasing influence of center-of-mass motion at higher

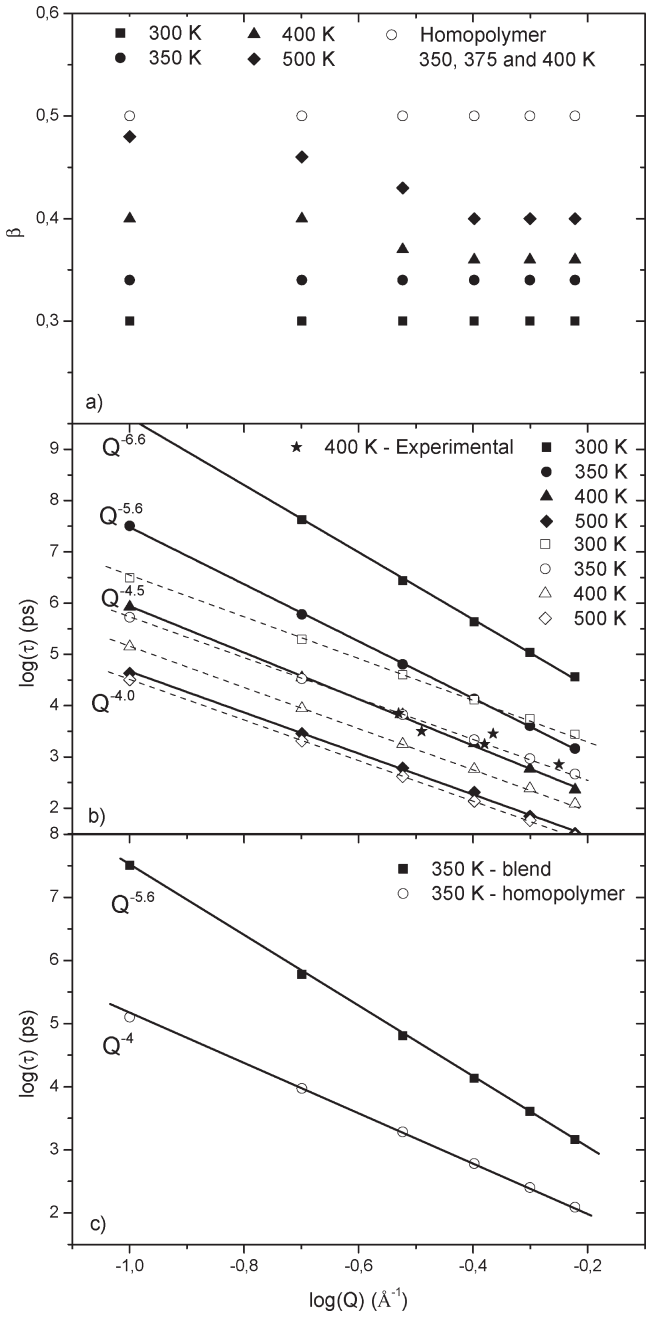

Figure 4. (a) β values at different Q values and temperatures arising from the KWW fits of the full incoherent scattering functions of PEO as homopolymer (empty symbols) and in the blend (full symbols) (b) Averaged τ for different Q values and temperatures for PEO in the blend. The full time-range and a variable β parameter were used for the full symbols, and the empty symbols show fits in the limited time windows with fixed $\beta = 0.5$. The stars show experimental results for $T = 400$ K for a blend composition of 25% PEO in 75% PMMA (BS-FZJ and IN16[17]). (c) For $T = 350$ K, comparison of the Q dependence of the average τ corresponding to the pure PEO (empty symbols) and PEO in the blend (filled symbols).

temperatures. We further note that the β values corresponding to $Q = 0.1$ Å^{-1} have a big uncertainty because the $F_s(Q,t)$ do not decay very much in the fitting range.

Figure 4b presents the Q dependence of the average relaxation time obtained from the full fits as well as in the restricted fitting regime corresponding to the neutron backscattering time window. As expected for Rouse-like behavior (Section IIIA), at 500 K, we find $<\tau(Q)> \propto Q^{-\gamma}$ with γ values close to 4. However, γ monotonically increases as the temperature decreases. Moreover, we note that $\gamma = 2/\beta$, indicating approximately Gaussian behavior in the intermediate long time regime, excluding times beyond 20 ns, where the plateau regimes become evident. This somewhat unexpected result may be rationalized in terms of our results for α_2. (See Figure 1c.) We know that values of α_2 lower than $\sim$0.2 approximately lead to Gaussian behavior of $F_s(Q,t)$.[53] Furthermore, at low Q, $F_s(Q,t)$ is particularly sensitive to long times where the non-Gaussian parameter is relatively low.

Concerning the restricted fits mentioned above, we recuperate the apparent Rouse-like Q^{-4} behavior, which again is a consequence of the approximate Gaussian behavior ($\gamma = 2/\beta$) and to the fact that in the considered time range, $\beta \simeq 0.5$. At high temperature, the restricted fits give basically the same Q dependence as the standard fits. This reflects the fact that at high temperature, the actual β value approaches 0.5 for the full relaxation function. Figure 4b also includes experimental data that were obtained by a procedure corresponding to the restricted fits. There is a reasonable agreement with these experimental data.

Finally, for a low temperature ($T = 350$ K), Figure 4c directly compares the Q dependence of the average relaxation times for pure PEO and PEO in the blend. The differences are evident without any type of analysis.

Figure 5a shows the temperature dependence of the average relaxation time corresponding to a Q value of 0.3 Å^{-1} for both PEO and PEO in the blend also including the result from the restricted fit. The restricted fit results apparently show the same activation energy as pure PEO; the average times are just shifted by a numerical factor. This finding agrees perfectly with the results obtained when experimental neutron (backscattering) data of PEO/PMMA for several compositions are fitted by using a Rouse expression for $F_s(Q,t)$.[49] The relaxation times corresponding to the full simulated relaxation function display significantly higher activation energies. We note that this again agrees well with experiments. If we take experimental data from neutron spin echo, which covers a significantly larger time regime than the backscattering data (t_{max} of $\sim$100 ns compared with $\sim$1 ns), a change of the activation energy from about 3300 to 6300 K is found, which is in good agreement with the simulations.

Finally, Figure 5b presents the temperature dependence of the β parameter for the same $Q = 0.3$ Å^{-1} in comparison with the power law parameter, x, describing the time dependence of the H-MSD as well as that of the center of mass. For pure PEO, the validity of the Rouse model is demonstrated ($\beta = 0.5$ and $x = 0.5$); for the center of mass, the simulations for pure PEO give x values on the order of 0.85 in agreement with experiment and simulations on other polymers.[54,55] In the case of the blend, the x parameter corresponding to the center of mass of the PEO chains takes values close to those of the homopolymer at high temperatures (low dynamic asymmetry) and strongly decreases with temperature, reflecting the increase in dynamic asymmetry in the system. For PEO/PMMA, β as well as the H-MSD exponent x decrease in parallel, with decreasing temperature indicating the approximate Gaussian behavior in the time regime where β was evaluated.

B. Bead−Spring Asymmetric Model. The results described in the previous section show that the large-scale dynamics of nonentangled PEO in the PEO/PMMA blend deviates from the Rouse behavior followed by pure PEO. These deviations become stronger as soon as the temperature decreases, and thereby the dynamic asymmetry between PEO and PMMA increases. Now the emerging question is whether the results obtained are particular for the PEO/PMMA system or

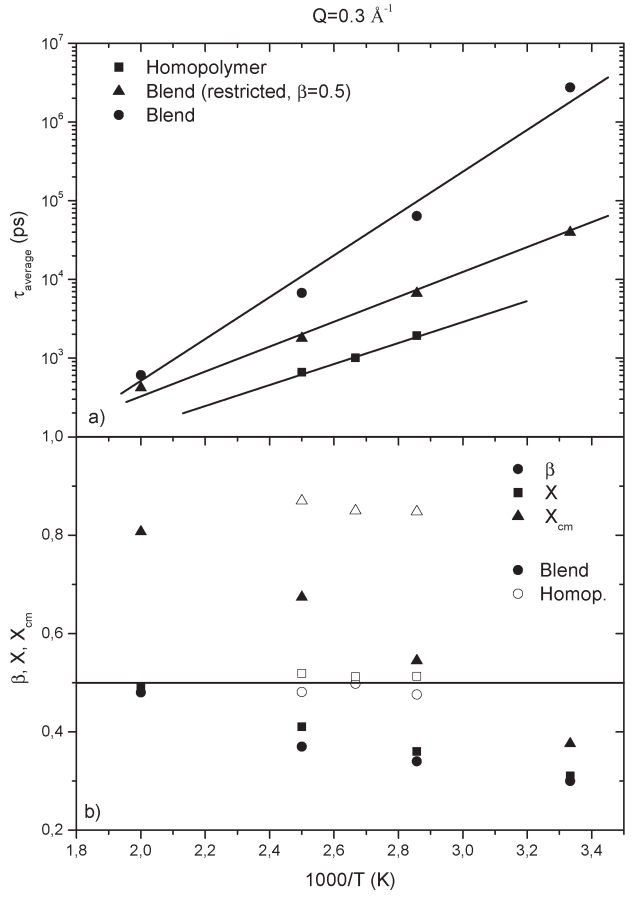

Figure 5. (a) Temperature dependence of $\tau_{average}$ for $Q = 0.3$ Å^{-1}. Results for the PEO homopolymer (■), PEO in the blend with restricted fitting windows (▲), and PEO in the blend with normal fitting procedure (●) are shown. (b) Temperature dependence of β values at $Q = 0.3$ Å^{-1} and slopes of the mean square displacement for the PEO as homopolymer (empty symbols) and the blend (filled symbols) at different temperatures.

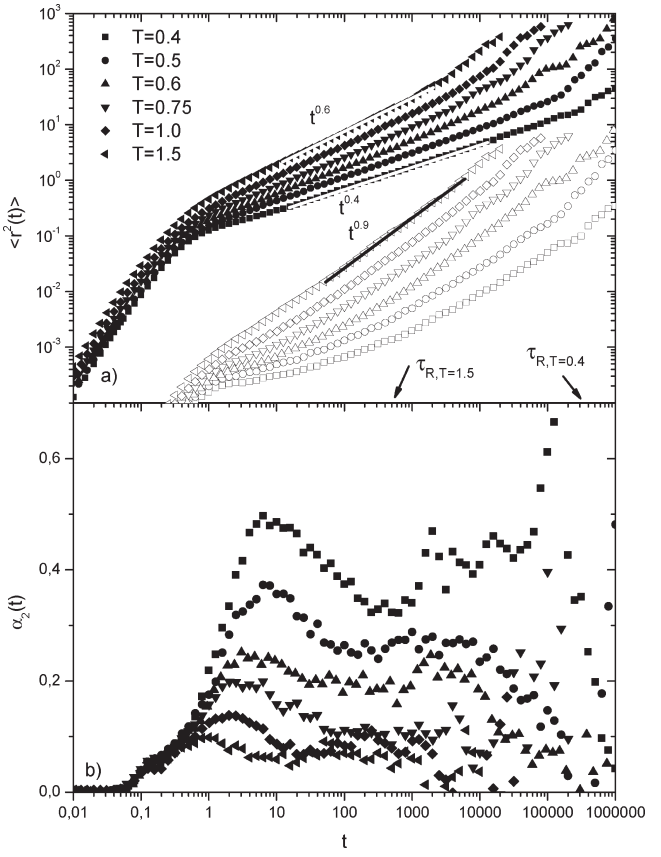

Figure 6. (a) Mean square displacement of the B component of the bead−spring blend for temperatures between 0.4 and 1.5. The MSD of the beads is shown as filled symbols. The MSD of the chain center of mass (empty symbols) has been shifted by a factor of 1/100. The lines show fits to power-laws with the corresponding exponents. (b) Non-Gaussianity parameter for the B beads in the blend.

generic results for dynamically asymmetric polymer blends. To answer this question, we can compare the results corresponding to PEO/PMMA with those obtained for general models as, for instance, bead−spring models.[31] These minimal models aim to retain some of the basic ingredients of chemically distinct systems to capture their relation to universal features observed in such systems. The explicit basic ingredients exhibited by the bead−spring blend model described in Section IIB and which are also present in the PEO/PMMA system are a strong dynamic asymmetry and short chain length (i.e., nonentangled chains). Previous simulations[30,31] on this model have shown that for low monomer concentrations (less than ∼35%) of the B component, the latter shows characteristic times, both for the structural α-relaxation and for chain dynamics, that are several decades faster than those for the A component. Therefore, the B component of the bead−spring blend plays the role of the PEO in the PEO/PMMA blends.

Figure 6a shows the monomer (bead) mean squared displacement, MSD, at different temperatures for the fast component B of the bead−spring polymer blend. The Rouse time is indicated in the Figure for some temperatures. It is noteworthy that the parameters of the bead−spring potential were chosen in such a way that the characteristic time scale of this model, which is measured in units of $\sigma_{BB}(m/\varepsilon)^{1/2}$ (Section II) approximately matches the time scale in picoseconds of the atomistic simulations. The length unit σ_{BB} roughly corresponds to a typical Kuhn length in real systems because the bead−spring chains have no internal barriers and are fully flexible.

As can be seen in Figure 6a, the qualitative behavior of the bead-MSD for the fast component B is similar to that obtained for PEO in the PEO/PMMA blend. (See Figure 1a.) In the time range between the microscopic dynamics and the Rouse time, the bead-MSDs display a power law increase $< r^2(t) > \approx t^x$, with x values ranging from ∼0.6 at high temperature to ∼0.4 at low temperature. These values display a similar trend as those from the atomistic simulations but are systematically higher. It is noteworthy that the high-T exponent, 0.6, for the B component in the blend is the same observed at all temperatures (not shown) in our simulations of the B homopolymer for this model, and in general, for similar models of nonentangled homopolymers.[56] In the case of the MSD corresponding to the center of mass of the chains, the behavior obtained is also qualitatively similar to that displayed by PEO in the blend. At high temperatures, we recover the behavior corresponding to the pure B component (x of the order of 0.9), and as the temperature decreases (dynamic asymmetry between A and B component increases), the value of x diminishes. However, we note that the lower values of x obtained are higher than those obtained in the case of the c.m. of PEO chains in the blend. This is likely due to the differences in chain length and also possibly to different quantitative values of dynamic asymmetry between both systems. Because of the faster dynamics of the c.m., we are able to observe in the bead

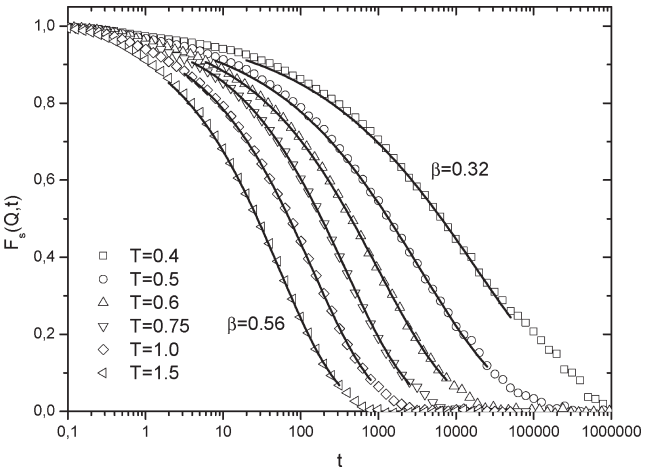

Figure 7. For the B component in the blend, dynamic incoherent scattering functions for $Q = 1.13$ at different temperatures. Lines are fits using KWW functions.

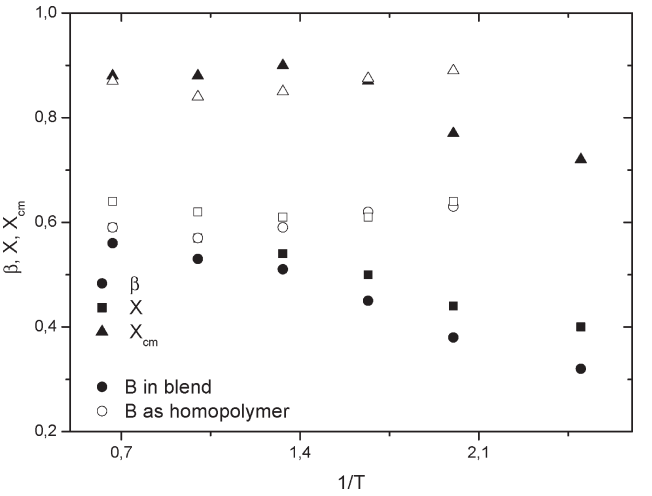

Figure 8. For the B component, temperature dependence of β values from KWW fits of the incoherent scattering functions, power-law exponents of the mean square displacement (x), and of the center-of-mass motion (x_{cm}). Filled symbols are data for B in the blend. Empty symbols are data for the B homopolymer.

MSD the crossover toward a diffusive-like regime at longer times ($t > \tau_R$), although the statistics in this range are rather poor. This regime is not observed in the case of atomistic simulations, where simulation times are shorter (about one decade) than in the case of the bead−spring simulations.

In Figure 6b, we show the behavior of the associated non-Gaussianity parameter $\alpha_2(t)$. In this case, because of the simplicity of the model, $\alpha_2(t)$ does not show the microscopic peak that is observed in fully atomistic models at ~0.1 ps. Apart from that, the behavior of $\alpha_2(t)$ is qualitatively rather similar to that displayed by PEO in the blend. $\alpha_2(t)$ develops a strong peak in the intermediate time range with a maximum value increasing as temperature decreases. This peak is followed by a broad, almost flat, regime with a level also increasing as the temperature decreases. However, it seems that this plateau vanishes at longer times (except maybe for the lowest temperature $T = 0.4$, note the poor statistics at long times) where the crossover toward the diffusive regime takes place. Obviously, this long-time behavior of $\alpha_2(t)$ cannot be observed in the case of PEO in PEO/PMMA because that crossover does not occur in the simulated time.

Figure 7 shows the incoherent scattering function $F_s(Q,t)$ for the fast B component as a function of the temperature for a low Q value ($Q = 1.13$) roughly equivalent to 0.3 $Å^{-1}$ in the case of PEO. Again, we observe a similar behavior as in the case of PEO in the blend. (See Figure 3a.). The stretching of $F_s(Q,t)$ increases as the temperature decreases and the dynamic asymmetry increases. At high temperature, the corresponding β parameter reaches values on the order of those for the homopolymer case (see below), whereas at the lowest temperature simulated, it takes a value on the order of 0.3 (same as PEO in the blend). Following the same procedure as in the case of PEO, we have fitted $F_s(Q,t)$ by KWW functions. A summary of the results obtained for $Q = 1.13$ at the different temperatures is shown in Figure 8, in comparison with the corresponding results for the pure B component. We observe the same qualitative trend with temperature as in the case of PEO in the blend. (See Figure 5b.) Moreover, here the β values do not depend on Q in the low-Q range and in the whole temperature range.

In conclusion, we can say that the results obtained for PEO in the blend PEO/PMMA seem to be generic for asymmetric polymer blends and that the deviations from Rouse-like behavior are driven by the temperature dependence of the dynamic asymmetry of the system. In the next section, the dynamics of both PEO in the PEO/PMMA blend and the B component in the bead−spring blend will be directly analyzed in terms of the Rouse coordinates and Rouse mode correlators.

V. Rouse Analysis of the Simulation Results

For the lower Rouse modes, the simulation results on an equivalent 43 monomer pure PEO melt revealed an excellent agreement with the predictions of the Rouse model.[41] This concerned: (1) the dependence of the mode relaxation time on the mode index p: $\tau_p \approx p^{-2}$, (2) the decrease in the mode amplitudes with the mode index $\langle X_p(0)^2 \rangle \approx p^{-2}$, and (3) the approximately single exponential line shape of the mode correlators.

For higher p (larger than ~10), deviations from the predictions of the Rouse model were systematically found for all of these quantities: (i) τ_p decays slightly stronger than p^{-2}, (ii) the line shape displays significant stretching ($\beta \approx 0.7$), and (iii) the mode amplitudes fall very significantly below the p^{-2} law. From a discussion in terms of the all rotational state (ARS) model, it was concluded that the main reason for these deviations appears to be a mode-dependent friction counteracting the stronger restoring forces at high p.

To rationalize the changes that the PMMA matrix imposes on the PEO dynamics, we performed a Rouse analysis on the present simulation results, both the atomistic MD as well as those on the coarse-grained bead spring model.

We commence with the fully atomistic MD simulations. To calculate the Rouse modes from the fully atomistic simulations melt, some coarse graining was performed in connecting several atoms to create one bead. As for the case of the pure PEO, we take the center of mass of one monomer as one bead creating 43 modes ($0 \le p \le 42$; the simulated PEO consists of 43 monomers). First, we test the precondition for a Rouse mode analysis, namely, the question of whether the Rouse modes are still reasonable eigenmodes of the "confined" PEO chains. Figure 9 presents the results. Here we display the amplitudes of the normalized mode correlators

$$\Phi_{pq}(t = 0) = \left\langle \frac{X_p(0)X_q(0)}{|X_p(0)||X_q(0)|} \right\rangle$$

for different temperatures. To give the full picture, we have plotted them versus an x variable constructed as $x = 42(p - 1) + q$.

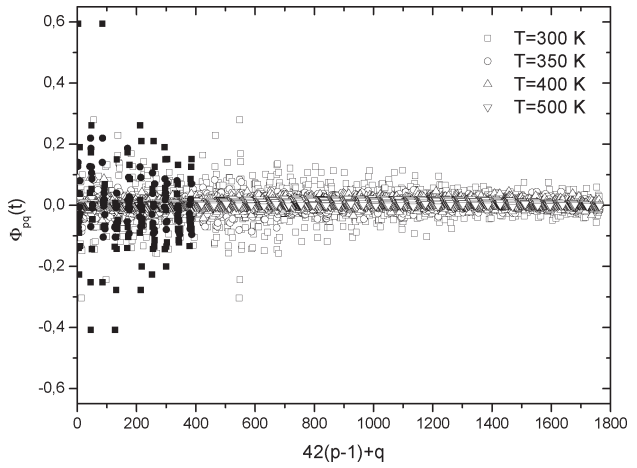

Figure 9. Mode correlators $\Phi_{pq}(0)$ normalized to the absolute values of the normal coordinates. To show all correlations, the values on the x axis are $x = 42(p-1) + q$. For $p = q$, the correlators are 1, and other values should be significantly smaller in case of Rouse behavior. For $T = 300$ and 350 K, large values are found for low values of q and p.

For $p = q$, all correlators are equal to one by construction. For temperatures $T > 350$ K, values below 0.1 are observed, and the orthogonality of the Rouse modes is confirmed, as we have found in the case of the pure PEO. For $T = 350$ and 300 K, significant deviations are found for correlators with low indices of p and q. (Values where p and q are < 10 are shown in full symbols at these temperatures.) For $T = 350$ K, only very few points with $\Phi_{pq}(0) > 0.1$ are found. At 300 K, about half of all values are > 0.1. They are mainly caused by bad statistical sets of the normal coordinates where the spatial configurations exploited by the chains at these low temperatures are very limited resulting in "bad" normal modes.

Figure 10a displays the time-dependent Rouse mode correlators Φ_{pp} for a selected set of mode numbers p at $T = 400$ K. The data are fitted with a stretched exponential describing their decay in all cases allowing quite a good description. Figure 10b compares selected correlators with those from the pure PEO melt. To facilitate this comparison, we have shifted the modes from the pure PEO by the ratio of the corresponding Rouse times $\tau_R^{PEO/PMMA}/\tau_R^{PEO} = 6.8$, such that the correlators for the first mode display the same relaxation time. We note: (i) the first mode of both systems displays a rather similar line shape; (ii) the higher mode correlators for the blend are significantly more stretched than those from pure PEO; and (iii) the spacing between the mode relaxation times $\tau_p^{PEO/PMMA}$ appears to be significantly larger than that for the pure melt. Because of this phenomenon, in Figure 10b, the higher modes in the blend appear to decay faster than those in the pure case. Figure 10c presents the temperature dependence of the mode $p = 5$ in the blend including a fit with a stretched exponential. For each case, the stretching parameter is indicated. With increasing temperature, we observe a strong decrease in the relaxation time, which is accompanied by a systematically reduced stretching.

Figure 11a,b,c shows the dependence of the average relaxation time $\langle\tau\rangle = \tau_W\Gamma(1/\beta)/\beta$, the stretching parameter β, and the mode amplitudes $\langle X_p(0)^2\rangle$ in dependence of the wavelength of the modes, N/p, and temperature. For some temperatures, the results from the pure PEO melt are also included. Whereas for the lower modes in the PEO melt, temperature-independent scaling $\langle\tau\rangle \approx p^{-2}$ is revealed (Figure 11a), a qualitatively different behavior is found for the blend: with decreasing temperature, the power law for the characteristic times displays an increasing exponent from $p^{-2.2}$ at $T = 500$ K to $p^{-2.7}$ at $T = 350$ K. For $T = 300$ K, the fit of a power law was not possible because of the high statistical

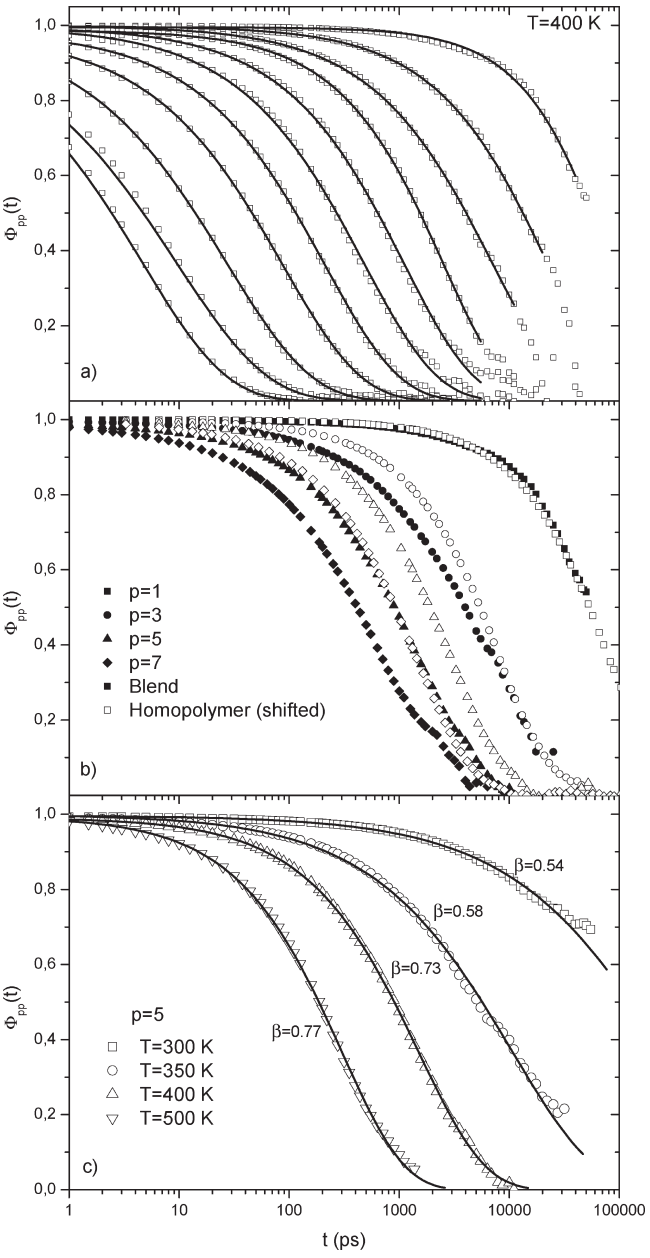

Figure 10. (a) Rouse mode correlators for PEO in the blend at 400 K, for $p = 1$, 2, 3, 4, 6, 8, 11, 15, 22, 30, and 40 with fits (lines) of stretched exponential functions. (b) Rouse mode correlators at 400 K for $p = 1$, 3, 5, and 7. The empty symbols are data for the PEO-homopolymer that have been shifted by the ratio of the Rouse times of the PEO-homopolymer and of PEO in the blend. (c) Rouse mode correlators for PEO in the blend ($p = 5$) at different temperatures with KWW fits (lines).

errors of the Rouse times. The corresponding relaxation times of the stretched exponential functions exceed the windows of the simulation (100 ns) by far. Toward higher mode numbers, the difference between the blend and the pure melt diminishes; for the highest p, basically identical values appear. PMMA is not significantly disturbing the PEO segmental motion very locally for wavelengths in the order of the bead size. Figure 11b also shows the stretching parameter as a function of N/p and temperature: (1) As in the pure melt (data included for $T = 350$ K), the blend data show a systematic decrease in β with increasing mode number. (2) Whereas for the melt this behavior does not depend on temperature, for the blend, the stretching parameter decreases strongly with decreasing temperature. However, it seems that the general dependence on the mode number is

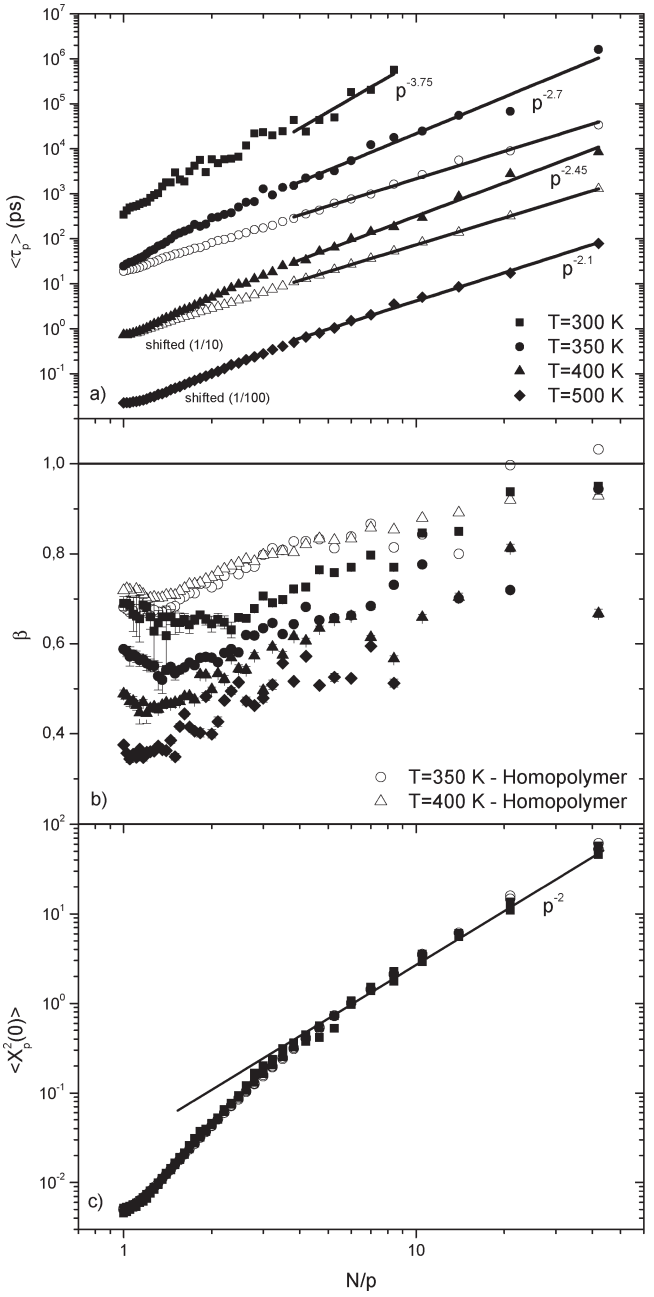

Figure 11. (a) Full symbols: average Rouse times $<\tau_p>$ as obtained from KWW fits for T = 300, 350, 400, and 500 K for PEO in the blend. Also included are data for the PEO-homopolymer at T = 350 and 400 K (empty symbols). Values for T = 400 and 500 K have been shifted by a factor of 0.1 and 0.001 for clarity. The Rouse times for the modes p = 1−4 have been removed for T = 300 K because they significantly exceeded the total simulations length. (b) Stretching parameter β at different temperatures, as obtained from KWW fits of the Rouse correlators. Empty and full symbols are data for, respectively, pure PEO and PEO in the blend. (c) Rouse amplitudes $<X_p^2(0)>$ for all temperatures of PEO in the blend and in the homopolymer. The results of the homopolymer (empty symbols) are hidden by the full symbols of the blend. No differences are found.

maintained. For lower modes, the stretching is always less pronounced than for higher modes. (3) Although the average relaxation times for the blend and the melt approach each other for high p, the stretching for the blend is significantly stronger, revealing a significant influence of the PMMA matrix also at short wavelengths. (4) With the exception of the 500 K simulation, the decay of the correlators for the lowest modes in the blend is not sufficient to reveal accurate β values. (5) Even at 500 K,

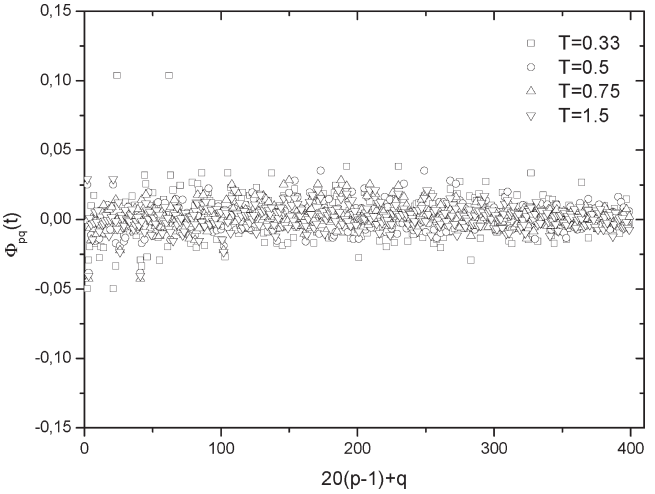

Figure 12. Mode correlators $\Phi_{pq}(0)$ normalized to the absolute values of the normal coordinates for the B component in the bead spring model. Values on the x axis are $x = 20(p-1)+q$.

where the blend H-MSD nearly follows a $t^{0.5}$ power law, the mode stretching at intermediate p is still significantly strong in comparison with that of the pure PEO melt. This suggests that even at this temperature, the PMMA matrix still has some influence on the PEO dynamics.

Finally, Figure 11c displays the mode amplitudes. We are confronted with an interesting result: for all temperatures, even where the PEO dynamics is significantly altered, we observe almost identical mode amplitudes as in the pure melt. Because the mode amplitude is directly related to the restoring forces for a given mode, we are led to the conclusion that the PMMA matrix is basically acting through increased friction, whereas it does not modify the acting forces in a noticeable way. Figure 11c also shows that the amplitudes of the Rouse correlators (chain static properties) follow the mode number scaling (p^{-2}) expected from Gaussian statistics on the larger length scales ($N/p > 5$). Obviously, on short length scales, our chains cannot be ideal because of the local potentials, in particular, the angular potential. This is shown by the deviations from the Rouse scaling. (See Figure 11c). The approach to coarse-grain one monomer as one single bead already implies these deviations for the higher modes. These results obtained from the Rouse analysis are in agreement with the values close to 6 for the ratio $<R_{ee}^2>/<R_g^2>$ (representative of larger scales), which were independently calculated from the simulation results (Table 1) and commented on in Section IIA. As soon as the temperature decreases and the dynamic asymmetry increases, however, the chain conformation of PEO slightly deviates from Gaussian statistics. For the lowest temperature, a ratio of 7.1 is found, hinting at stretched PEO chains. Recent results by small-angle neutron scattering in PEO/PMMA seem to confirm this trend [D. Schwahn, private communication].

Concerning the bead−spring polymer blend here considered, we have followed a similar analysis in terms of Rouse correlators as that carried out for PEO/PMMA simulations. For the case of the B component in the bead−spring blend, which has no intramolecular barriers leading to local stiffness, the assumption of Gaussianity is expected to be a good approximation, except for very local length scales. (See below.) In Figure 12, we present the corresponding values of $|\Phi_{pq}(t = 0)|$ for the B component. (Now we do not distinguish between low and high modes in the representation). Similarly to the MD simulations, the x axis is chosen to present all correlations; this time, only modes 1−20 are available because the chain contains 21 beads. Almost all of the off-diagonal terms are < 0.1, and essentially all Rouse modes can be considered to be "good" normal modes.

Figure 13 summarizes the results obtained focusing on the fast component B, equivalent to PEO in the atomistic system. Figure 13a shows the wavelength N/p dependence of the average relaxation time $<\tau_p>$ at the different temperatures simulated. We observe the same behavior as that shown in Figure 11a for PEO in the blend. For the low modes, we obtain $\tau_p \approx p^{-x}$ with x_p values depending on temperature and ranging from ~2.2 at high temperature (as in the case of pure B component for all temperatures) to ~3.5 at the lowest temperature simulated. Figure 13b displays the stretching parameter β also as a function of N/p for three representative temperatures covering the full range investigated. Again, we note that the β values strongly depend on temperature for the fast B component in the blend. The nonexponentiality of the Rouse correlators in this case dramatically increases as the temperature decreases. Figure 13b also shows that this is not the case for the pure B homopolymer. As in the case of pure PEO, the β values corresponding to low and high temperatures nicely overlap within the data scattering. We note that the β values corresponding to the pure B homopolymer also match the values of the B component in the blend at high temperature. Finally, the amplitudes of the different Rouse modes are represented in Figure 13c for both the pure B homopolymer and the B component in the blend and for different temperatures. As for PEO, we observe identical amplitudes in both situations. Finally, only the behavior in the high mode number range is different for PEO and B. This is obviously due to the fact that the bead−spring model does not incorporate local potentials that are the responsible for the behavior displayed by PEO in this range. It is worthy of remark that similar results were previously reported[31] for simulations of bead−spring models of asymmetric polymer blends of different chain-lengths, always in the range of nonentangled systems.

We can conclude that also in terms of detailed Rouse analysis, the results obtained for PEO in PEO/PMMA blend are rather generic for asymmetric polymer blends.

VI. Discussion

The Rouse model neglects spatial and time correlations of the stochastic forces, that is

$$\langle f_\alpha(n,t) f_\beta(m,0)\rangle = 2k_B T\zeta_0\, \delta_{nm}\, \delta_{\alpha\beta}\, \delta(t)$$

This approximation yields orthogonality and exponential relaxation of the Rouse correlators. Orthogonality is a consequence of the uncorrelation between the forces at different positions and exponentiality of the uncorrelation of the forces at different times. In fact, orthogonality and exponentiality of the Rouse correlators are the two main ingredients of the Rouse model and the basis for the predictions for chain dynamics.

The results reported here for PEO in PEO/PMMA blend and, in general, for the fast component in dynamically asymmetric polymer blends[31], show that even though orthogonality can be considered as a reasonable approximation, the shape of the Rouse correlators strongly deviates from exponentiality. This is evidence that the assumption of time uncorrelation of the stochastic forces breaks down for the fast component, in particular, as the temperature decreases, and thereby the dynamic asymmetry between the two components of the blend increases. This dynamic asymmetry implies that the chains of the fast component are moving in a matrix where the density fluctuations are relaxing with a characteristic time, which increases as temperature decreases and may reach infinity at the slow component T_g. As has been described in Section III, several theoretical approaches based on projector operator techniques incorporate density fluctuations around the tagged chain within a memory kernel in a generalized Langevin equation (GLE).[36−38] Slow relaxation of the memory kernel induces nonexponential behavior of the Rouse modes in qualitative agreement with the results reported here. The Rouse model (pure exponential behavior) is recovered as a particular case for which density fluctuations around the tagged chain relax on a microscopic time scale. In asymmetric polymer blends, this situation will be reached in the limit of high temperature where the dynamic asymmetry of both

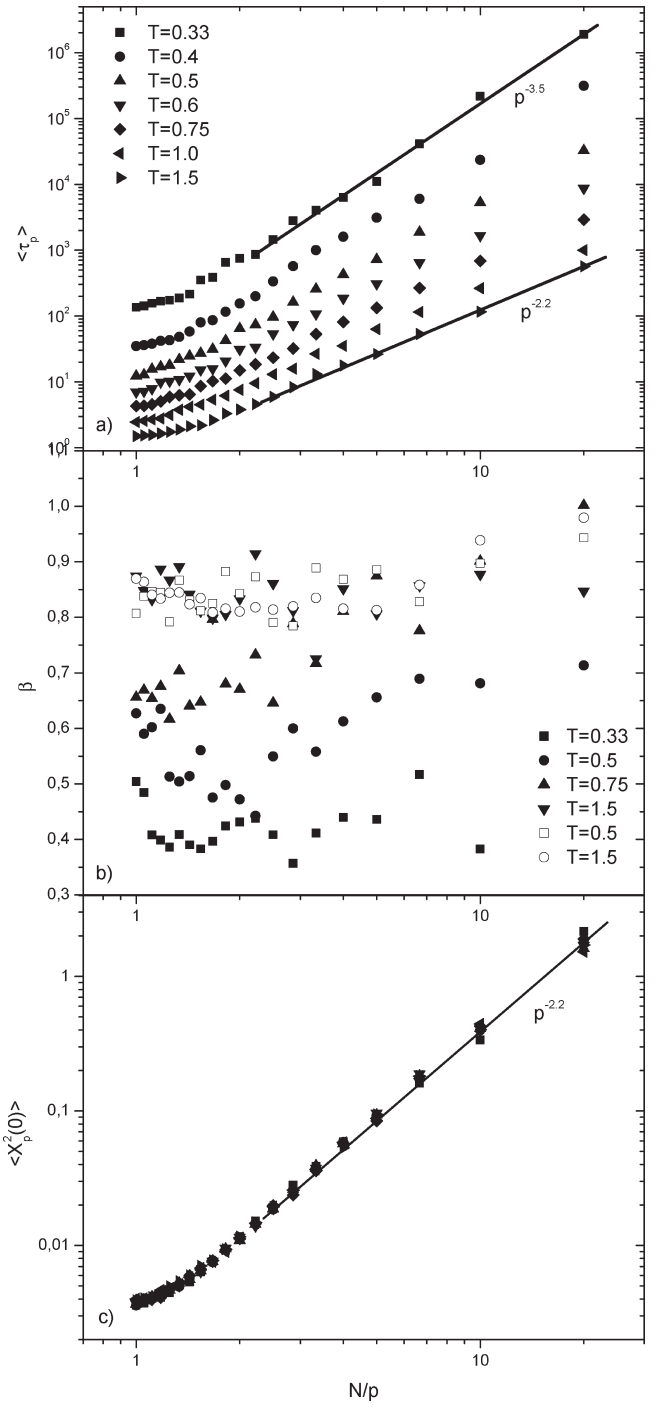

Figure 13. (a) Rouse times $<\tau_p>$ for the B component in the bead−spring model at all temperatures. As the temperature decreases, the exponent changes similarly to the simulations on PEO/PMMA. (b) β values at different temperatures, as obtained from KWW fits on the time-dependent Rouse correlators. Empty and filled symbols are data for, respectively, the B homopolymer and B in the blend. (c) Rouse amplitudes for different temperatures of the bead spring model. All points fall on top each other, as was observed for the simulations on PEO/PMMA (Figure 11c).

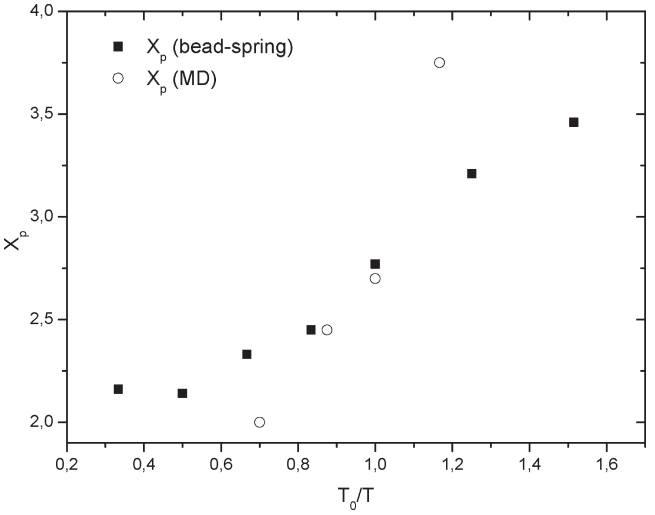

Figure 14. Temperature dependence of the exponent, x_p, which is obtained from fits of power laws to the Rouse times $<\tau_p>$. As the temperature decreases, a crossover from 2.0 (Rouse model) to higher values is observed both in PEO/PMMA (empty symbols) and in the bead−spring model (full symbols).

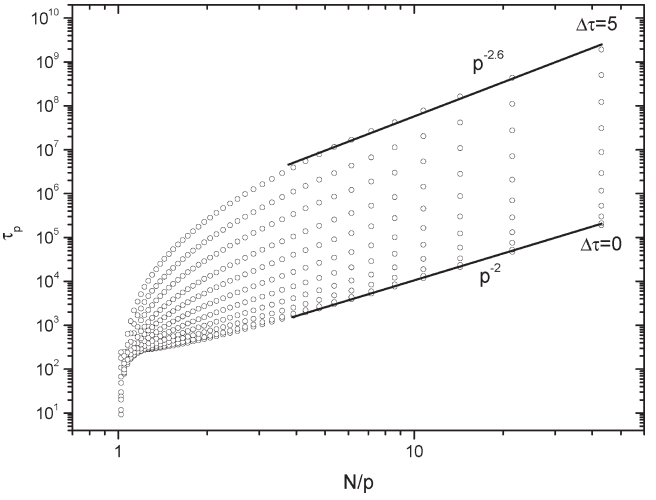

Figure 15. $<\tau_p>$ as calculated using the random Rouse model (log-normal distribution of friction coefficients) for an increasing distribution width, $\Delta\tau$. The exponent x_p increases from 2.0 to higher values, and the Rouse time is shifted several orders of magnitudes to higher values.

blend components vanishes. This nicely explains why at high temperature the dynamics of the fast component approaches that corresponding to the pure component, that is, the Rouse behavior characteristic of a nonentangled polymer.

Such GLE models were developed to describe the effect of increasing molecular weight (chain-length) on chain dynamics, that is, for the crossover between nonentangled Rouse dynamics to well-entangled chain dynamics. These methods through approximations of the memory kernel within the so-called renormalization Rouse models (Section III), predict for τ_p, other than pure reptation, where a second N^3/p^2 regime appears, a crossover from $(N/p)^2$ toward an $(N/p)^{x_p \leq 3.5}$ dependence by increasing the chain length. Such a crossover has been observed in simulations of entangled homopolymers.[33−35] As was pointed in ref 31, a similar crossover is induced for the fast (nonentangled) component in asymmetric polymer blends by increasing the dynamic asymmetry, that is, by decreasing temperature. Figure 14 nicely shows an example of such a crossover for the studied bead−spring system. The Figure also shows that when the data of x_p are represented on a normalized temperature scale, the PEO in PEO/PMMA data also follow a similar trend as the fast B component in the bead−spring blend model, although the temperature dependence is much steeper. The GLE methods also predict a concomitant crossover for the mean squared displacement behavior $<r^2(t)> \approx t^x$. The x-parameter crossing over from ∼0.5 to ∼0.3 has been demonstrated in Figure 1. However, as has also been mentioned in Section III, the precise values of the exponents (x, x_p, β) depend on the approximations made for the memory kernel (the so-called renormalization procedure).

The results for the two systems investigated here clearly show that the amplitudes of the Rouse modes for the fast component in the blend remain the same as for the pure components; that is, the restoring forces are not affected by the matrix at any temperature. From a qualitative point of view, this result suggests the picture of a time-dependent friction affecting the fast-component monomers. Moreover, as temperature decreases and the matrix is becoming more and more frozen, we should also expect the development of strong spatial heterogeneities, which eventually would produce additional distributions of the friction coefficient. We could expect that the influence of these heterogeneities on the chain dynamics would be stronger in the low temperature limit, where the density fluctuations of the matrix (slow-component) are just frozen. The random Rouse model introduced in Section III is in fact based on the idea of a distribution of friction coefficients due to these heterogeneities for the case of slowly fluctuating or frozen density fluctuations of the slow matrix. As displayed in Section III, the model has the advantage that it provides semianalytic solutions, allowing an explicit calculation of the structure factor. The random Rouse model was introduced for describing the single-chain dynamic structure factor of PEO measured by neutron spin echo (NSE) techniques on PEO/PMMA blends of different compositions. In that case and because of the high molecular weight of both components, the time scale of the density fluctuations of PMMA matrix was several orders of magnitude slower than PEO dynamics in the range investigated. Under these conditions, the random Rouse model showed to be a reasonable approximation for describing the chain dynamics of PEO in the blends. Now we can try to see whether the random Rouse model is able to reproduce the low-p asymptotic p-dependence of τ_p found in both bead−spring and PEO-PMMA simulations.

For that purpose, we need to calculate τ_p in the framework of the random Rouse model with some distribution of the friction coefficients. By analogy to the procedure followed to analyze the above-mentioned experimental data, we choose log-normal distributions of the following form

$$f(\zeta, \zeta_0, \sigma) = \frac{1}{\zeta\sigma\sqrt{2\pi}} \exp\left[-\frac{(\ln(\zeta) - \ln(\zeta_0))^2}{2\sigma^2}\right]$$

The width parameter σ was varied, and ζ_0 was kept constant. On the order of 1000 chains were considered in the calculations. Random frictions sampled from the corresponding distribution were associated with beads of these chains, and τ_p was calculated and averaged (43 monomers were assumed as in the MD-simulations of PEO/PMMA). The results for different values of $\Delta\tau = \sqrt{2}\sigma$ (ranging from 0 to 5 in steps of 0.5) are shown in Figure 15. For low values of $\Delta\tau$, τ_p follows the typical p^{-2} behavior with deviations at high p values because of the finite chain size. As the width of the friction distribution increases (the average friction was kept constant), lower modes experience a strong increase in relaxation times. Single beads with large friction coefficients slow down the movement of the whole chain and therefore slow down the low modes. Higher modes are not

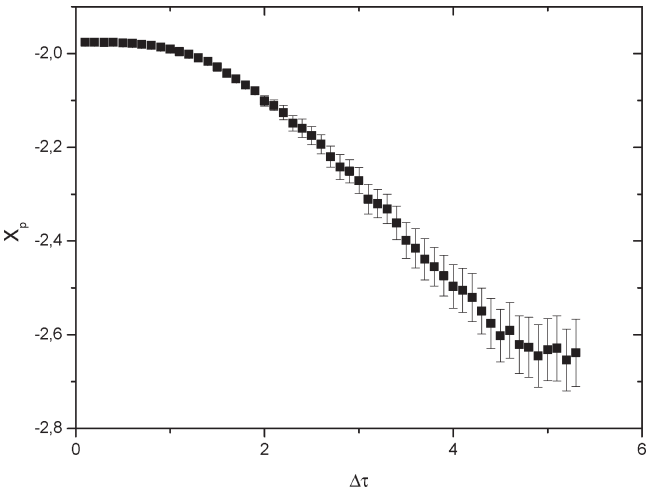

Figure 16. Change of the exponent, x_p, with the distribution width, $\Delta\tau$, as obtained from the random Rouse model.

strongly affected by these immobilized beads, agreeing with the findings in the simulations. Under these conditions, the N/p dependence of τ_p shows a bending to low values as N/p decreases. Fitting a power law to the asymptotic low-p (high N/p) range is possible and provides the changes of the exponent in $\tau_p \propto p^{-x}$ and facilitates a comparison of these exponents with those obtained from the MD simulations. Figure 16 shows the dependence of x_p with the width of the distribution. For low distribution-widths, exponents close to 2 are obtained, as expected for systems with about constant friction. As the width increases, the exponent increases as well, reaching an asymptotic value of ~2.6. Therefore, qualitatively, the random Rouse model would also be able to reproduce the changes of x_p as the temperature decreases by assuming a temperature-dependent distribution of friction coefficients. The maximum values of x_p that can be obtained (on the order of 2.6) are close to those obtained in the PEO/PMMA system at T = 350 K and slightly lower than those for the bead−spring simulations (~3.0). The exact values strongly depend on the p range that is used for the fitting of the power law. However, for comparable values of x_p the corresponding shift of the relaxation times at low p values is much larger than that found in the simulations. For instance, at 350 K, the Rouse time τ_R of PEO in the PEO/PMMA simulations shifts from ~30 ns in the homopolymer to 1700 ns in the blend, a factor of 55. To produce the same power law exponent x_p using the random Rouse model, the width of the friction distribution needs to be very large, $\sigma \approx 5$. Then, the random Rouse model predicts a shift of the longest relaxation time by a factor of about 10 000, much beyond the simulation results.

The reason for this discrepancy is that the random Rouse model assigns constant friction coefficients to each bead, which do not change with time. A chain is severely slowed down by beads with very high frictions. In the MD simulations, it is evident that the local environment fluctuates, and beads that are immobilized with high friction at one point in the simulation could be released from their blocked position after the environment has relaxed and then are allowed to move. This process, which is nicely captured by the models based on memory function formalisms, is not possible in the random Rouse model. Having noted this, the above-mentioned shift predicted by the random Rouse model is in good agreement with the findings of Haley and Lodge,[32] who find a corresponding shift of the diffusion coefficient for extreme dilution of PEO in a glassy matrix of PMMA. This result suggests that the random Rouse model can be a reasonable description for mobile chains in a nonrelaxing matrix.

VII. Conclusions

Chain dynamics of unentangled PEO in dynamically asymmetric PEO/PMMA blends strongly deviate from the Rouse behavior observed in pure PEO melts of similar molecular weight. These deviations are evident not only in the low-Q behavior of the intermediate scattering function and MSD but also directly in the evolution of Rouse correlators.

The behavior of PEO in PEO/PMMA is similar to that observed in general bead−spring models of asymmetric polymer blends, thereby indicating that these are generic features of dynamically asymmetric blends and not particular for the PEO/PMMA system.

The deviations from the Rouse model are driven by the dynamic asymmetry − different mobility of both components in the blend − of the system. Such deviations are stronger as temperature decreases and thereby the dynamic asymmetry increases.

The generic features summarized above can be understood in terms of GLE models which, although developed for a different problem, namely, the effect of increasing molecular weight on the chain dynamics, seem to be well-suited for describing the effect of slow density fluctuations of the matrix component of the blend on the chain dynamics of the unentangled fast component.

The random Rouse model appears to be a reasonable description of the system but is not fully applicable to the results of the presented simulations because it only describes the limiting case of extreme dynamic asymmetry, that is, mobile chains in a nonrelaxing matrix.

Acknowledgment. This research project was supported by the European Commission NoE SoftComp under contract no. NMP3-CT-2004-502235 and the "Donostia International Physics Center." F.A. and J.C. acknowledge support from projects MAT2007-63681 and IT-436-07 (GV) and the Spanish Ministerio de Educacion y Ciencia (grant no. CSD2006-53). A.J.M. acknowledges project 2007-60I021. M.B. thanks NoE SoftComp for support through the Eurothesis project.

References and Notes

(1) Colmenero, J.; Arbe, A. Segmental dynamics in miscible polymer blends: recent results and open questions. *Soft Matter* **2007**, *3*, 1474–1485.
(2) Maranas, J. K. The effect of environment on local dynamics of macromolecules. *Curr. Opin. Colloid Interface Sci.* **2007**, *12*, 29–42.
(3) Chung, G. C.; Kornfield, J. A.; Smith, S. D. Component dynamics miscible polymer blends: a two-dimensional deuteron NMR investigation. *Macromolecules* **1994**, *27*, 964–973.
(4) Chung, G.-C.; Kornfield, J. A.; Smith, S. D. Compositional dependence of segmental dynamics in a miscible polymer blend. *Macromolecules* **1994**, *27*, 5729–5741.
(5) Alegria, A.; Colmenero, J.; Ngai, K. L.; Roland, C. M. Observation of the component dynamics in a miscible polymer blend by dielectric and mechanical spectroscopies. *Macromolecules* **1994**, *27*, 4486–4492.
(6) Zawada, J. A.; Ylitalo, C. M.; Fuller, G. G.; Colby, R. H.; Long, T. E. Component relaxation dynamics in a miscible polymer blend: poly(ethylene oxide)/poly(methyl methacrylate). *Macromolecules* **1992**, *25*, 2896–2902.
(7) Arbe, A.; Alegría, A.; Colmenero, J.; Hoffmann, S.; Willner, L.; Richter, D. Segmental dynamics in poly(vinylethylene)/polyisoprene miscible blends revisited. A neutron scattering and broadband dielectric spectroscopy investigation. *Macromolecules* **1999**, *32*, 7572–7581.
(8) Lodge, T. P.; McLeish, T. C. B. Self-concentrations and effective glass transition temperatures in polymer blends. *Macromolecules* **2000**, *33*, 5278–5284.
(9) Leroy, E.; Alegría, A.; Colmenero, J. Segmental dynamics in miscible polymer blends: modeling the combined effects of chain connectivity and concentration fluctuations. *Macromolecules* **2003**, *36*, 7280–7288.

(10) Lodge, T. P.; Wood, E. R.; Haley, J. C. Two calorimetric glass transitions do not necessarily indicate immiscibility: the case of PEO/PMMA. *J. Polym. Sci., Part B: Polym. Phys.* **2006**, *44*, 756–763.

(11) Leroy, E.; Alegría, A.; Colmenero, J. Quantitative study of chain connectivity inducing effective glass transition temperatures in miscible polymer Blends. *Macromolecules* **2002**, *35*, 5587–5590.

(12) Lorthioir, C.; Alegría, A.; Colmenero, J. Out of equilibrium dynamics of poly(vinyl methyl ether) segments in miscible poly(styrene)/poly(vinyl methyl ether) blends. *Phys. Rev. E* **2003**, *68*, 031805.

(13) Genix, A. C.; Arbe, A.; Alvarez, F.; Colmenero, J.; Willner, L.; Richter, D. Dynamics of poly(ethylene oxide) in a blend with poly(methyl methacrylate): a quasielastic neutron scattering and molecular dynamics simulations study. *Phys. Rev. E* **2005**, *72*, 031808.

(14) Lutz, T. R.; Yiyong, H.; Ediger, M. D.; Cao, H.; Lin, G.; Jones, A. A. Rapid poly(ethylene oxide) segmental dynamics in blends with poly(methyl methacrylate). *Macromolecules* **2003**, *36*, 1724–1730.

(15) Brosseau, C.; Guillermo, A.; Cohen-Addad, J. P. NMR observation of poly(ethylene oxide) dynamics in a poly(methyl methacrylate) matrix: effect of chain length variation. *Macromolecules* **1992**, *25*, 4535–4540.

(16) Lartigue, C.; Guillermo, A.; Cohen-Addad, J. P. Proton NMR investigation of the local dynamics of PEO in PEO/PMMA blends. *J. Polym. Sci., Part B: Polym. Phys.* **1997**, *35*, 1095–1105.

(17) Niedzwiedz, K.; Wischnewski, A.; Monkenbusch, M.; Richter, D.; Genix, A.-C.; Arbe, A.; Colmenero, J.; Strauch, M.; Straube, E. Polymer chain dynamics in a random environment: heterogeneous mobilities. *Phys. Rev. Lett.* **2007**, *98*, 168301.

(18) Sakai, V. G.; Chen, C.; Maranas, J. K.; Chowdhuri, Z. Effect of blending with poly(ethylene oxide) on the dynamics of poly(methyl methacrylate): a quasi-elastic neutron scattering approach. *Macromolecules* **2004**, *37*, 9975–9983.

(19) Farago, B.; Chen, C.; Maranas, J. K.; Kamat, S.; Colby, R. H.; Pasquale, A. J.; Long, T. E. Collective motion in poly(ethyleneoxide)/poly(methylmethacrylate) blends. *Phys. Rev. E* **2005**, *72*, 031809.

(20) Tyagi, M.; Arbe, A.; Alegría, A.; Colmenero, J.; Frick, B. Dynamic confinement effects in polymer blends. A quasielastic neutron scattering study of the slow component in the blend poly(vinyl acetate)/poly(ethylene oxide). *Macromolecules* **2007**, *40*, 4568–4577.

(21) Urakawa, O.; Ujiia, T.; Adachi, K. Dynamic heterogeneity in a miscible poly(vinyl acetate)/poly(ethylene oxide) blend. *J. Non-Cryst. Solids* **2006**, *352*, 42–49.

(22) Genix, A.-C.; Arbe, A.; Arrese-Igor, S.; Colmenero, J.; Richter, D.; Frick, B.; Deen, P. P. Neutron scattering investigation of a diluted blend of poly(ethylene oxide) in polyethersulfone. *J. Chem. Phys.* **2008**, *128*, 184901.

(23) Kopf, A.; Dünweg, B.; Paul, W. Dynamics of polymer "isotope" mixtures: molecular dynamics simulation and Rouse model analysis. *J. Chem. Phys.* **1997**, *107*, 6945–6955.

(24) Kamath, S.; Colby, R. H.; Kumar, S. K. Dynamic heterogeneity in miscible polymer blends with stiffness disparity: computer simulations using the bond fluctuation model. *Macromolecules* **2003**, *36*, 8567–8573.

(25) Faller, R. Correlation of static and dynamic inhomogeneities in polymer mixtures: A computer simulation of polyisoprene and polystyrene. *Macromolecules* **2006**, *39*, 462.

(26) Luettmer-Strahmann, J.; Mantina, M. Local and chain dynamics in miscible polymer blends: A Monte Carlo simulation study. *J. Chem. Phys.* **2006**, *124*, 174907.

(27) May, A. F.; Maranas, J. K. The single chain limit of structural relaxation in a polyolefin blend. *J. Chem. Phys.* **2006**, *125*, 024906.

(28) Bedrov, D.; Smith, G. D. A molecular dynamics simulation study of segmental relaxation processes in miscible polymer blends. *Macromolecules* **2006**, *39*, 8526–8535.

(29) Sacristán, J.; Chen, C.; Maranas, J. K. Role of effective composition on dynamics of PEO-PMMA blends. *Macromolecules* **2008**, *41*, 5466–5476.

(30) Moreno, A. J.; Colmenero, J. Is there a higher-order mode coupling transition in polymer blends? *J. Chem. Phys.* **2006**, *124*, 184906.

(31) Moreno, A. J.; Colmenero, J. Entangledlike chain dynamics in nonentangled polymer blends with large dynamic asymmetry. *Phys. Rev. Lett.* **2008**, *100*, 126001.

(32) Haley, J. C.; Lodge, T. P. Dynamics of a poly(ethylene oxide) tracer in a poly(methyl methacrylate) matrix: remarkable decoupling of local and global motions. *J. Chem. Phys.* **2005**, *122*, 234914.

(33) Schaffer, J. S. Effects of chain topology on polymer dynamics: configurational relaxation in polymer melts. *J. Chem. Phys.* **1995**, *103*, 761.

(34) Kremer, K.; Grest, G. S. Dynamics of entangled linear polymer melts: A molecular-dynamics simulation. *J. Chem. Phys.* **1990**, *92*, 5057.

(35) Padding, J. T.; Briels, W. J. Time and length scales of polymer melts studied by coarse-grained molecular dynamics simulations. *J. Chem. Phys.* **2002**, *117*, 925.

(36) Kimmich, R.; Fatkullin, N. Polymer chain dynamics and NMR. *Adv. Polym. Sci.* **2004**, *170*, 1–113.

(37) Schweizer, K. S. Microscopic theory of the dynamics of polymeric liquids: general formulation of a mode−mode-coupling approach. *J. Chem. Phys.* **1989**, *91*, 5802.

(38) Schweizer, K. S.; Fuchs, M.; Szamel, G.; Guenza, M.; Tang, H. Polymer-mode-coupling theory of the slow dynamics of entangled macromolecular fluids. *Macromol. Theory Simul.* **1997**, *6*, 1037–1117.

(39) Sun, H. Ab initio calculations and force field development for computer simulation of polysilanes. *Macromolecules* **1995**, *28*, 701–712.

(40) Sun, H. COMPASS: an ab initio force-field optimized for condensed-phase applicationsoverview with details on alkane and benzene compounds. *J. Phys. Chem. B* **1998**, *102*, 7338–7364.

(41) Brodeck, M.; Alvarez, F.; Arbe, A.; Juranyi, F.; Unruh, T.; Holderer, O.; Colmenero, J.; Richter, D. Study of the dynamics of poly(ethylene oxide) by combining molecular dynamic simulations and neutron scattering experiments. *J. Chem. Phys.* **2009**, *130*, 094908.

(42) Theodorou, D. N.; Suter, U. W. Atomistic modeling of mechanical properties of polymeric glasses. *Macromolecules* **1986**, *19*, 139–154.

(43) Theodorou, D. N.; Suter, U. W. Local structure and the mechanism of response to elastic deformation in a glassy polymer. *Macromolecules* **1986**, *19*, 379–387.

(44) Martuscelli, E.; Silvestre, C.; Luisa Addonizio, M.; Amelino, L. Phase structure and compatibility studies in poly(ethylene oxide)/poly(methyl methacrylate) blends. *Makromol. Chem.* **1985**, *187*, 1557–1571.

(45) Tanis, I.; Karatasos, K. Local dynamics and hydrogen bonding in hyperbranched aliphatic polyesters. *Macromolecules* **2009**, *42*, 9581–9591.

(46) Frenkel, D.; Smit, B. *Understanding Molecular Simulation: From Algorithms to Applications*; Academic Press: San Diego, CA, 1996.

(47) Rouse, P. E. A theory of the linear viscoelastic properties of dilute solutions of coiling polymers. *J. Chem. Phys.* **1953**, *21*, 1272.

(48) McLeish, T. C. B. Tube theory of entangled polymer dynamics. *Adv. Phys.* **2002**, *51*, 1379–1527.

(49) Niedźwiedź, K. Polymer dynamics in miscible polymeric blends. Ph.D. Thesis, University of Münster, **2007**.

(50) Doi, M.; Edwards, S. F. *The Theory of Polymer Dynamics*; Clarendon Press: Oxford, U.K., 1988.

(51) Smith, G. D.; Paul, W.; Monkenbusch, M.; Willner, L.; Richter, D.; Qiu, X. H.; Ediger, M. D. Molecular dynamics of a 1,4-polybutadiene melt: comparison of experiment and simulation. *Macromolecules* **1999**, *32*, 8857–8865.

(52) Zamponi, M.; Wischnewski, A.; Monkenbusch, M.; Willner, L.; Richter, D.; Falus, P.; Farago, B.; Guenza, M. G. Cooperative Dynamics in Homopolymer Melts: A Comparison of Theoretical Predictions with Neutron Spin Echo Experiments. *J. Phys. Chem. B* **2008**, *112*, 16220–16229.

(53) Colmenero, J.; Alvarez, F.; Arbe, A. Self-motion and the α-relaxation in a simulated glass-forming polymer: crossover from Gaussian to non-Gaussian dynamic behavior. *Phys. Rev. E* **2002**, *65*, 041804.

(54) Smith, G. D.; Yoon, D. Y.; Wade, C. G.; O'Leary, D.; Chen, A.; Jaffe, R. L. Dynamics of poly(oxyethylene) melts: comparison of ^{13}C nuclear magnetic resonance spin-lattice relaxation and dielectric relaxation as determined from simulations and experiments. *J. Chem. Phys.* **1997**, *106*, 3798.

(55) Smith, G. D.; Paul, W.; Monkenbusch, M.; Richter, D. A comparison of neutron scattering studies and computer simulations of polymer melts. *Chem. Phys.* **2000**, *261*, 61–74.

(56) Bennemann, C.; Paul, W.; Binder, K.; Dünweg, B. Molecular-dynamics simulations of the thermal glass transition in polymer melts: α-relaxation behavior. *Phys. Rev. E* **1998**, *57*, 843–851.